



Article

Investigating the Surface Damage to Fuzhou's Ancient Houses (Gu-Cuo) Using a Non-Destructive Testing Method Constructed via Machine Learning

Lei Zhang ^{1,2}, Yile Chen ² , Liang Zheng ^{2,*} , Binwen Yan ¹, Jiali Zhang ¹, Ali Xie ¹ and Senyu Lou ^{2,3}

¹ School of Civil Engineering and Architecture, Wuyi University, No. 358 Baihua Road, Wuyishan 354300, China; zhanglei@wuyiu.edu.cn (L.Z.); 18396581213@163.com (B.Y.); 19005082646@163.com (J.Z.); 19559990679@163.com (A.X.)

² Faculty of Humanities and Arts, Macau University of Science and Technology, Avenida Wai Long, Tapai, Macau 999078, China; 2009853gat30001@student.must.edu.mo (Y.C.); 20161018@jhc.edu.cn (S.L.)

³ Architectural Engineering Institute, Jinhua University of Vocational Technology, Jinhua 321000, China

* Correspondence: 2009853gat30002@student.must.edu.mo

Abstract: As an important part of traditional Chinese architecture, Fuzhou's ancient houses have unique cultural and historical value. However, over time, environmental factors such as efflorescence and plant growth have caused surface damage to their gray brick walls, leading to a decline in the quality of the buildings' structure and even posing a threat to the buildings' safety. Traditional damage detection methods mainly rely on manual labor, which is inefficient and consumes a lot of human resources. In addition, traditional non-destructive detection methods, such as infrared imaging and laser scanning, often face difficulty in accurately identifying specific types of damage, such as efflorescence and plant growth, on the surface of gray bricks and are easily hampered by diverse surface features. This study uses the YOLOv8 machine learning model for the automated detection of two common types of damage to the gray brick walls of Fuzhou's ancient houses: efflorescence and plant growth. We establish an efficient gray brick surface damage detection model through dataset collection and annotation, experimental parameter optimization, model evaluation, and analysis. The research results reveal the following. (1) Reasonable hyperparameter settings and model-assisted annotation significantly improve the detection accuracy and stability. (2) The model's average precision (AP) is improved from 0.30 to 0.90, demonstrating good robustness in detecting complex backgrounds and high-resolution real-life images. The F1 value of the model's gray brick detection efficiency is improved (classification model performance index) from 0.22 to 0.77. (3) The model's ability to recognize the damage details of gray bricks under high-resolution conditions is significantly enhanced, demonstrating its ability to cope with complex environments. (4) The simplified data enhancement strategy effectively reduces the feature extraction interference and enhances the model's adaptability in different environments.

Keywords: non-destructive detection; machine learning; surface damage; architectural heritage; Fuzhou City



Citation: Zhang, L.; Chen, Y.; Zheng, L.; Yan, B.; Zhang, J.; Xie, A.; Lou, S. Investigating the Surface Damage to Fuzhou's Ancient Houses (Gu-Cuo) Using a Non-Destructive Testing Method Constructed via Machine Learning. *Coatings* **2024**, *14*, 1466. <https://doi.org/10.3390/coatings14111466>

Academic Editors: Antonina Chaban, Jana Striova and Rita Deiana

Received: 25 October 2024

Revised: 12 November 2024

Accepted: 16 November 2024

Published: 18 November 2024



Copyright: © 2024 by the authors. Licensee MDPI, Basel, Switzerland. This article is an open access article distributed under the terms and conditions of the Creative Commons Attribution (CC BY) license (<https://creativecommons.org/licenses/by/4.0/>).

1. Introduction

In the Fuzhou dialect, “Gu-cuo” refers to ancient houses in a narrow sense and old buildings in a broad sense [1]. These houses include buildings with various functions, including city walls, artillery positions, temples, palaces, residential houses, and ancestral halls, all of which fall into the category of “ancient houses” [2,3]. White walls, dark tiles, curved gables, and cornices comprise the unique form and beauty of Fuzhou's ancient houses, and they are also iconic elements of Fujian architecture [4]. As a legally protected object in Fuzhou City, Fuzhou's ancient houses encompass all types of architectural heritage. Among the bricks, tiles, woods, and stones, we witness the passing of the years; the

memory of the city is contained within these structures, expressing a deep nostalgia. Since modern times, the ancient houses in Fuzhou have emerged in relation to such star-studded romantic figures as Lin Zexu, Yan Fu, Shen Baozhen, and Lin Juemin, and they are filled with the feelings of family and country and the conveyance of poetry and calligraphy across generations, as well as farming and reading [1,5]. This is not only the birthplace of local culture but also the continuation of an important architectural heritage. Fuzhou is among the country's second batch of historical and cultural cities, as well as one of the first ten pilot cities for the protection and utilization of historical buildings. Fuzhou boasts a wealth of cultural relics and historic sites and a profound cultural heritage [6]. In 1997, Fuzhou took the country's lead in promulgating and implementing the "Regulations on the Protection of Fuzhou Historical and Cultural Cities", laying a solid foundation for Fuzhou's legislative protection of historical and cultural cities [7]. So far, the Fuzhou Ancient Houses Group has restored more than 300 ancient houses in historical and cultural districts such as Sanfang Qixiang (Three Lanes and Seven Alleys Historic District), Shangxiahang Historic District, and Liangcuo Historic District, with a total restoration area of nearly 400,000 m² [8,9]. With so many architectural heritage restoration and protection requirements, it has recently become possible to use machine learning technology to assist in surface damage identification.

The protection of architectural heritage is rapidly evolving in the new era of digital technology, with information technology, "Internet+", and artificial intelligence constantly emerging [10]. As historical city protection planning gains momentum, the conservation of Fuzhou's ancient architectural heritage urgently necessitates the integration of big data, networks, and cloud computing, underscoring the scientific approach to safeguarding Fuzhou's ancient buildings in the new era. Artificial intelligence technology has produced a non-destructive surface damage detection method for architectural heritage, replacing high-cost detection technologies such as radiographic testing (RT), ultrasonic testing (UT), liquid penetrant testing (PT), magnetic particle testing (MT), eddy current testing (ECT), acoustic emission testing (AE), thermal imaging/infrared (TIR), leakage test (LT), alternating current field measurement technology (ACFMT), magnetic flux leakage testing (MFL), the far-field testing method (RFT), and the ultrasonic diffraction time-of-flight method (TOFD), which can only achieve accurate detection when the object under test is a single body. It instead uses non-destructive and low-cost methods to train relevant software after obtaining materials through manual shooting so as to conduct a comprehensive detection of the surface details of gray bricks in ancient buildings, ensuring that accurate data are obtained without damaging the gray bricks themselves. Non-destructive testing techniques do not require physical contact or the destruction of building surfaces, reducing the potential damage to building structures. This provides a scientific basis for the protection and restoration of ancient buildings. The advanced technical means and the embodiment of the concept of cultural relics and monument protection not only reflect its scientific nature but also provide strong support for the inheritance and development of traditional architectural culture. This technology has broad application prospects and will surely play an increasingly important role in the future.

Numerous studies have been undertaken in the field of ancient houses in Fuzhou, with the majority focusing on qualitative analyses and in-depth investigations of the various components of these buildings [11–13]. However, when considering building materials, ancient craftsmen used a variety of non-renewable, characteristic, locally sourced materials. Models have been directly applied to identify existing road defects [14], road vehicles [15], foreign debris [16], eucalyptus wood [17], blueberries [18], and railway track surface defects [19]. It is challenging to align these models with the characteristics of traditional Fujian architecture. Therefore, this study aims to use YOLOv8 machine learning technology for image analysis. This technology can automatically identify different damage to the surface of Fuzhou's ancient houses' wall tiles, thereby reducing the labor costs, enhancing the maintenance of Fuzhou's ancient houses, and potentially contributing to the preservation of future ancient house historic districts. This article mainly focuses on three

key questions. (1) Based on on-site investigation and photography, what types of damage affect the brick walls of ancient houses in Fuzhou? (2) How effective is the trained machine learning model? (3) How accurate is the automatic detection identification?

2. Literature Review

2.1. Protection and Development of Traditional Fujian Architecture

Fuzhou's ancient houses are important residential buildings in Fujian and an important source of the cultural heritage of the region [20]. However, the rapid development of urbanization has put Fuzhou's ancient houses in danger of elimination, posing severe challenges to their survival and development. Fuzhou is an important city on the southeast coast of China, with rich cultural heritage resources [21]. It is a national historical and cultural city. Some scholars have explored the architectural heritage of Fuzhou City. For example, they collected data on cultural heritage sites in Fuzhou City and established a GIS database. They used cluster analysis, nearest neighbor analysis, buffer zone analysis, and other GIS methods to study the spatial distribution characteristics of cultural heritage in Fuzhou City [22,23]. These studies found that the temporal evolution and spatial distribution characteristics of cultural heritage are closely related to historical and cultural factors. They explored the impact mechanism of natural and human geographical factors on the distribution of cultural heritage in Fuzhou City and even the entire Fujian Province from a multi-scale and multi-type perspective, providing theoretical support and a data reference for the protection and development of local cultural heritage. Some scholars have also analyzed the layout, architectural components, enclosure form, settlement structure, spatial order, and other characteristics of traditional courtyard spaces in the Three Lanes and Seven Alleys Historic District of Fuzhou from the perspective of spatial morphology, based on the cultural background and regional characteristics of Fuzhou. They calculated the integration degree between the courtyard space units and the street space and used the space syntax to analyze the potential relationship between its spatial structure and social activities, such as connectivity, controllability, average depth, integration, comprehensibility, and synergy, and thus summarized the principles of the courtyard morphology [24]. Some scholars also hold the belief that the "living museum" of traditional dwellings in Fujian Province serves as a theory and method for the protection and renewal of historical blocks, drawing on the principles of ecological museums. The essence of the "living museum" is community renewal, adhering to the principle of people-orientedness, focusing on preserving the development trend of traditional architectural culture and transforming the protection of traditional buildings into a continuous process of renewal and development [25]. In addition, numerous scholars have proposed evaluation indicators or methods based on the renewal design and protection strategies of Fujian's traditional buildings, thereby promoting the protection and renewal of architectural heritage in the region [26–30]. These studies further demonstrate that Fujian's cultural heritage has received increasing attention and research from scholars.

2.2. Surface Technology for Architectural Heritage

The protection of architectural heritage is not only aimed at architectural spaces but also focuses on damage to the surface and technical strategies. Many studies, utilizing a combination of instruments and equipment, employed existing technologies to monitor the surface of architectural heritage buildings. For example, as early as 2005, Hemmleb et al. used RGB images of various resolutions and near-infrared images of different wavelengths and adopted the ISODATA algorithm to perform unsupervised classification to analyze the damage to brick wall sections [31]. In a subsequent study, Hemmleb et al. (2006) used two indices—the Normalized Difference Vegetation Index (NDVI) and the Normalized Difference Moisture Index (NDMI)—to clearly mark vegetated or wet areas on images [32]. Sidiropoulou-Velidou et al. used multi-temporal thermal imaging (rather than near-infrared images) combined with RGB images to detect the damage and reconstruction areas on stone exterior walls [33]. They collected one RGB image and four multi-temporal thermal images

as raw data and manually registered them using Adobe Photoshop. They then integrated these images into a seven-band image file, which subsequently formed a principal component analysis (PCA) file. They were classified into 14 categories using supervised maximum likelihood analysis. Finally, the diseased and remodeled areas were manually marked by overlapping the classified images with the thermal images and referring to the temperature differences at several points on the thermal images [33]. Meroño et al. (2015) performed laser scanning and used a digital SLR camera with multiple filters to capture images in the visible and near-infrared spectral range. They utilized ENVI software to register and analyze these images, employing object-oriented analysis to identify characteristic diseases of stone masonry walls. The analysis initially employed the watershed by immersion algorithm, followed by the K-nearest neighbor (KNN) algorithm at a later stage. Finally, the classification results were combined with the laser scanning point cloud to form a 3D model containing disease information [34]. The scholars Teza et al. (2013) developed a MATLAB toolbox that can use multi-phase thermal imaging to identify different materials and cracks in historical buildings. The toolbox contains algorithms for correcting, mosaicking, and registering thermal images, calculating thermal contrast, and identifying damage. They applied this tool to a brick bell tower damaged in an earthquake in Italy. They took five sets of thermal images of an exterior wall from a distance of about 50 m, achieving an image resolution of about 3.4 cm per pixel [35]. The test results successfully distinguished different materials or damaged areas, including repair materials, metals, and cracks. Del Pozo et al. (2015) used a phase-shift measurement laser scanner and two cameras to record the facades of historical buildings and divided them into six categories according to the materials and diseases: unmodified granite, modified granite, wood (doors), wet areas, mortar, and biological colonies. They believed that supervised classification is better suited to correctly distinguishing different types of materials and diseases [36]. In addition, Riveiro et al. proposed a method for automatically extracting stone contours in block stone masonry using laser scanning point clouds [37,38]. In addition, some scholars used fiber optics and wireless sensing technology to monitor ancient buildings. They transmitted the measurements taken at the building surface to the monitoring center for data processing and prediction, realizing comprehensive monitoring, reliable transmission, and intelligent processing, and building an intelligent information service system that connects people and things [39]. With the rise of artificial intelligence technology, it has become possible to identify damage to the surface of architectural heritage buildings. As mentioned above, the use of machine learning technology to identify objects [14–19] has been extended to various disciplines, but there is no dedicated model for regional architectural heritage buildings.

3. Materials and Research Process

3.1. Study Area

Founded in 306 B.C., Fuzhou boasts a rich history spanning over 2300 years [40]. It is the birthplace and source of prosperity of Fujian culture. The Chinese government listed it in the second batch of national historical and cultural cities in 1986 [41]. It has long been Fujian's political, economic, and political center. The State Council has approved it as one of the central cities in the West Coast Economic Zone, and it serves as a cultural and transportation center [42,43]. It is the headquarters of the Army Agency of the Eastern Theater Command of the Chinese People's Liberation Army. It is an important city on China's southeast coast, a marine economic development demonstration zone, the gateway to the Maritime Silk Road, and a component of the China (Fujian) Free Trade Pilot Zone. It was one of the first five treaty ports in modern China [44].

The ancient houses in Fuzhou are a type of residential building that closely aligns with the commercial culture and economic environment of the area. These unique residential buildings are primarily distributed in areas of Fuzhou with high economic development levels. Among them, Cangshan District, Gulou District, and Taijiang District are the three oldest administrative districts with the largest population density and the most prosperous economy. They are also the areas with the largest number of local residents and the largest

number of existing ancient houses. Therefore, this study primarily focuses on the three ancient urban areas of Fuzhou: Cangshan District, Gulou District, and Taijiang District (Figure 1).

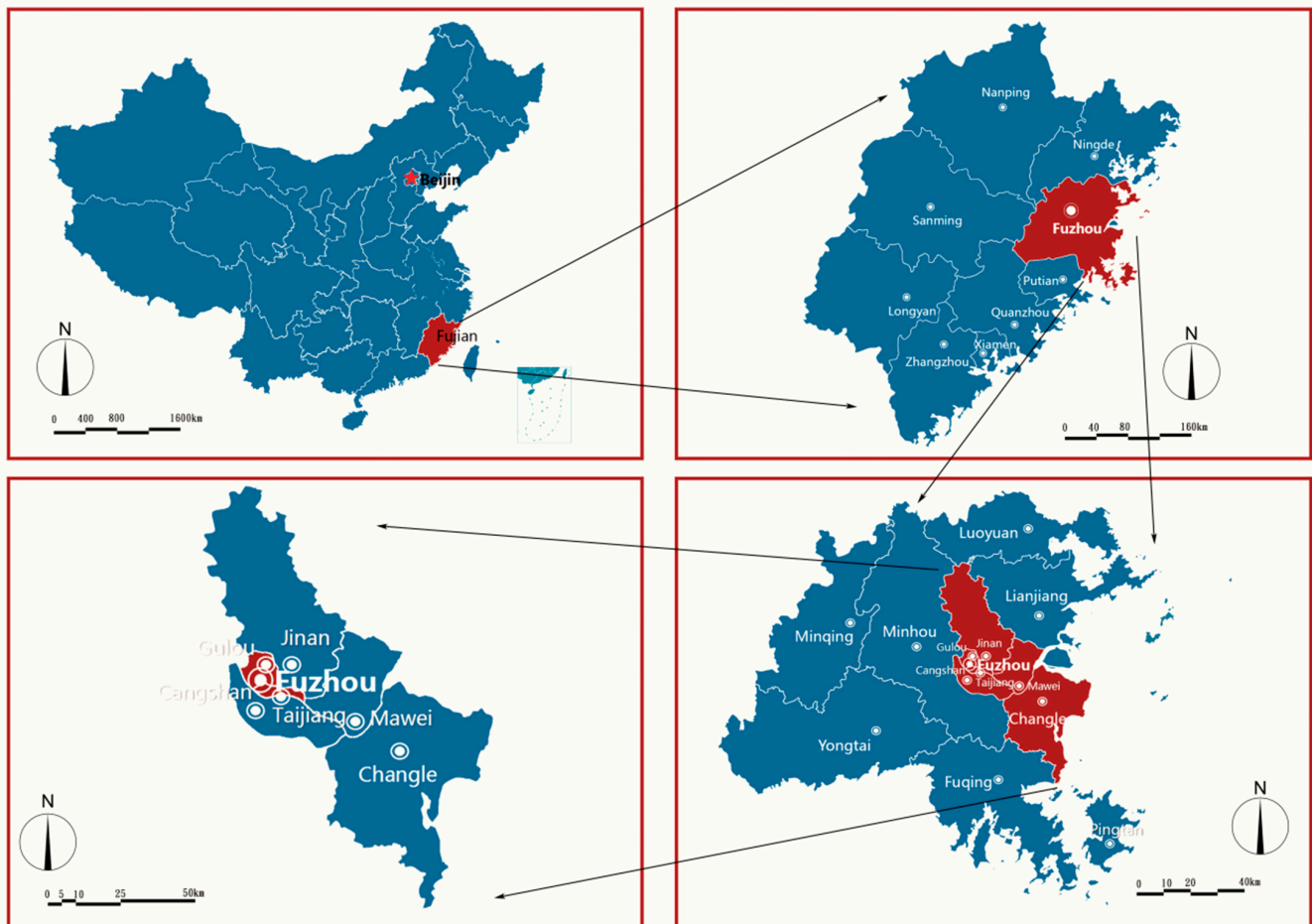


Figure 1. Scope of the research and investigation (image source: drawn by the author).

3.2. Image Collection Source: Selection of Buildings for Field Investigations

According to official statistics, the urbanization rate of Fuzhou City exceeded 60% in 2011, which was nearly 10% higher than the national average. Fuzhou has experienced rapid development in the past 30 years, particularly since its listing as a key development city in the West Coast Economic Zone of the Taiwan Straits in 2004. The most typical feature is the rapid expansion of urban construction land. As construction land expands around Fuzhou City, it also infiltrates into the historical blocks that feature the relatively intact old city style of Fuzhou. Fuzhou City comprises four main historical and cultural districts: Three Lanes and Seven Alleys Historic District, Zhuzifang Historic District, Shangxiahang Historic District, and Yantaishan Historic District. We selected research objects from the four aforementioned areas, selecting a total of 32 ancient houses from Fuzhou. The researchers collected data in May 2024 in order to obtain representative data suitable for use as standard samples. This was due to the following. (1) Suitable climatic conditions: The temperature and humidity in May are relatively moderate, which is conducive to the visualization of gray brick surface damage types (such as efflorescence and plant growth), avoiding the interference of hot and humid summer weather or cold and wet winter weather in the surface damage performance. For example, high temperatures and strong sunlight in summer will intensify plant growth, which may cause some more seriously damaged areas to be completely covered, affecting observations, while the cold and wet winter climate may make some minor damage difficult to observe. (2) Influence of seasonal changes: In May (late spring and early summer), vegetation grows actively but has not yet completely

covered a large area of the building surface. The efflorescence phenomenon of gray bricks is also more significant due to the suitable climate. This means that data from May more closely reflect the characteristics of various damage types, which is convenient for data diversity and model universality. (3) Data consistency: In order to ensure the stability and consistency of the data, selecting a fixed time period for collection reduces the interference caused by differences in climatic conditions in different months, thereby improving the training effect and applicability of the model. We collected an average of 30 photos per building, documenting the damage to the gray bricks on the main facade and other exposed facades (Figure 2). For details of the buildings, please refer to Appendix A.

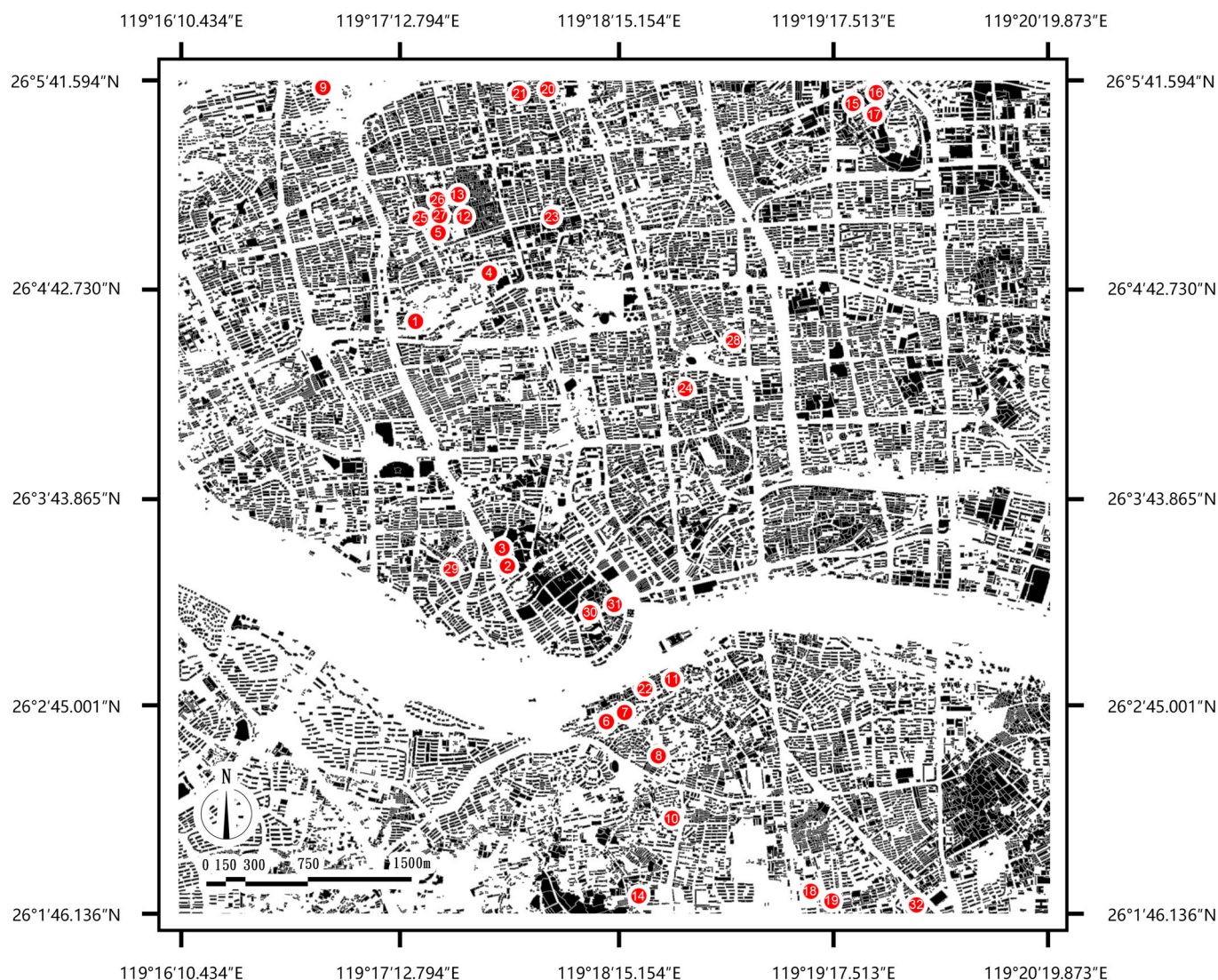


Figure 2. The locations where the photos were collected. The numbers in the figure represent the following: 1 is No. 108 Wushan Road; 2 is No. 151 Baima South Road; 3 is No. 169 Baima South Road; 4 is No. 17 Tianhuangling Lane; 5 is No. 20 Daguangli; 6 is No. 250 Dongguan Street; 7 is No. 254 Dongguan Street; 8 is No. 172 Heping Street; 9 is No. 44 Jing Street; 10 is Jiuyan Gong Dacuo; 11 is Kaiyinglu; 12 is No. 50 Nanhou Street; 13 is No. 174 Nanhou Street; 14 is Shangbao Qizhu Hall; 15 is No. 4 Weicuoli; 16 is No. 8 Weicuoli; 17 is the former residence of the Wei family; 18 is No. 135 Wushan Village; 19 is Wushan Mansion, Wushan Village; 20 is No. 1 Chiqian, Yijing Village; 21 is No. 9 Chiqian, Yijing Village; 22 is No. 11 Zhonglie Road; 23 is No. 50 Zhuzifang; 24 is No. 58 Taibaojing Lane; 25 is No. 6 Wenrufang; 26 is No. 42 Nanhou Street; 27 is No. 20 Daguangli; 28 is No. 2 Longjin Yizhi Lane; 29 is the former site of Yihua Photo Studio; 30 is No. 78–84 Zhongping Road; 31 is No. 88–98 Zhongping Road; and 32 is No. 53 Dongxing (image source: drawn by the author).

3.3. Research Methods and Process

This study took Fuzhou's ancient houses (Gu-cuo) as the research object and was divided into two parts: field investigation and automatic recognition model construction. First, comprehensive data collection related to the gray brick surfaces of these ancient houses was carried out, including their physical characteristics, environmental exposure conditions, and existing damage. At the same time, this study also included a preliminary analysis of the architectural structure, distribution location, and regional climate of gray brick buildings and Fuzhou's ancient houses. Second, the YOLOv8 model framework method was used to identify unique features related to the surface damage to gray bricks. YOLO (You Only Look Once) uses a neural network for real-time detection, so it has an extremely fast detection speed and good accuracy. Subsequently, based on the extracted features, the model was rigorously verified and calibrated using a large number of sample data from different ancient houses in Fuzhou. The established gray brick surface damage detection model can provide a scientific basis and technical support for the protection of Fuzhou's ancient buildings, facilitating more accurate assessments of the current state of the ancient houses and guiding more effective protection and restoration strategies.

The following seven steps were used to construct the model to detect gray bricks in Fuzhou's ancient houses (Figure 3). These steps are crucial to ensuring the scientificity and accuracy of the model and can effectively improve the efficiency and quality of architectural heritage protection.

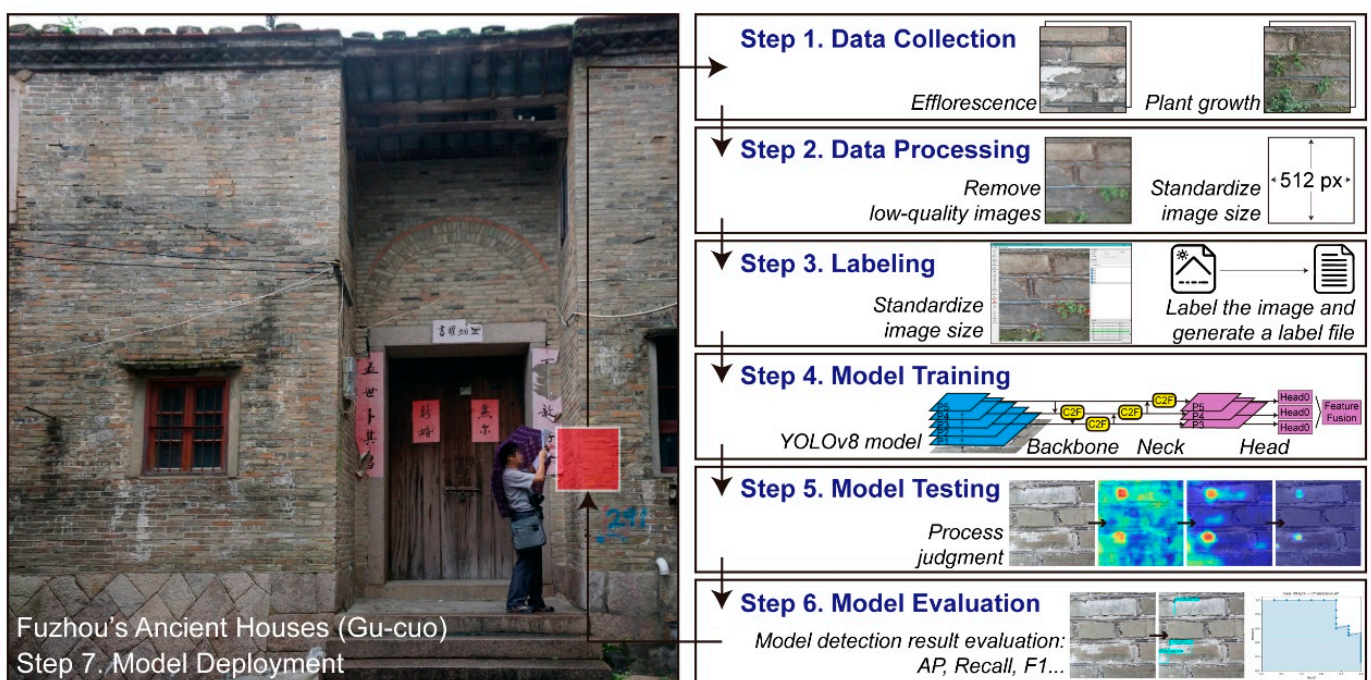


Figure 3. Research methods and steps (image source: drawn by the author).

(1) Data collection: This study collected a total of 556 high-resolution photos of gray bricks through field research. These photos were of 32 ancient houses in Fuzhou. We collected a total of 49 gray brick photos, excluding those with significant or minor problems, and identified two main types of damage in the photos: gray brick efflorescence and plant growth. The photos cover different weather, lighting, and environmental conditions to ensure data diversity.

(2) Data processing: This study standardized the collected images, including cropping, resizing, and contrast enhancement, to highlight the detailed features of gray brick. All the images were uniformly cropped to 512×512 pixels. The main purpose was to ensure a consistent image size, thereby reducing the complexity of the model input and improving

the model training efficiency and convergence speed. In addition, this cropping ensured the effectiveness of the model in terms of feature extraction and enhanced the learning ability concerning gray brick surface details. At the same time, some blurred and unclear images were eliminated to avoid interference with model training, thereby improving the overall performance of the model. Next, we divided the large image into multiple small pieces to enhance the data volume and boost the model training efficiency. Additionally, we used data enhancement techniques like rotation, flipping, and brightness adjustment to expand the dataset, thereby enhancing the model's generalization ability.

(3) Data labeling: This study used the LabelImg tool to label the collected images [45,46] (Figure 4). The LabelImg tool is installed in the created computer operating environment through the prompt command. At the same time, the LabelImg tool allows for viewing created annotations, correcting existing annotations, and even creating new annotations. Researchers can also delete the most incorrect annotations as needed, create new annotations, or adjust annotations with minor errors. The labeled gray brick damage types included efflorescence and plant growth. The quality of the annotations on the dataset directly influences the machine learning. Errors in the annotations will lead to poor machine learning. This is because the ability of the neural network to detect a given object depends on what it has learned. If we annotated something incorrectly or ambiguously, i.e., taught it the wrong object, the neural network would reflect this. In order to improve the accuracy of the model training, this research team not only used multiple rounds of verification and modification on the labeled data but also used model-assisted labeling (MAL). This method can improve the efficiency of labeling, reduce human labeling errors, and optimize the labeling results through continuous iteration of the model, thereby further improving the accuracy and robustness of the model. These labeled data involved a total of 49 images, ensuring the learning effect of the model under different damage scenarios.

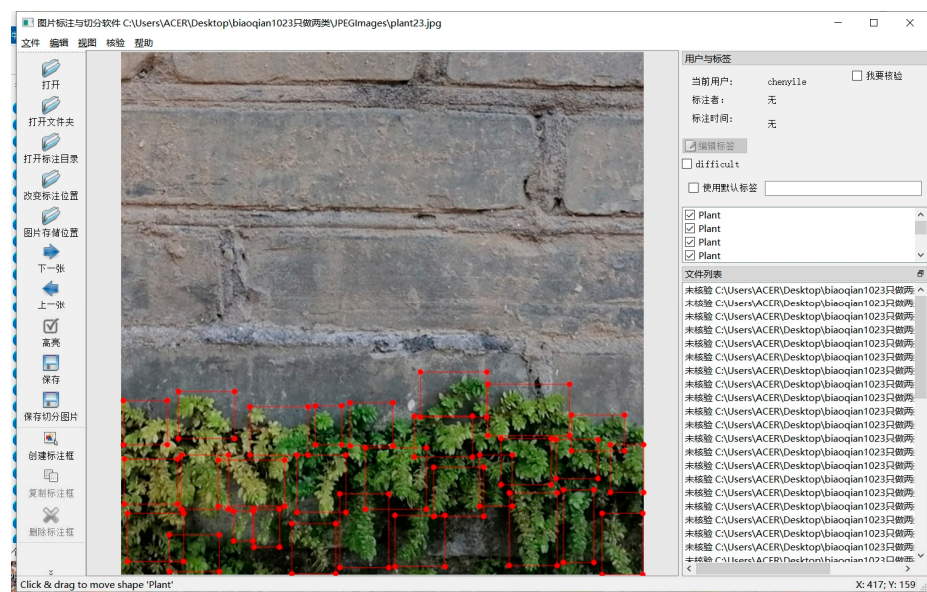


Figure 4. We used the LabelImg tool to label the collected images. Since the author uses the simplified Chinese version of the software, the Chinese displayed in the screenshot is that which comes with the LabelImg tool. The red box in the figure represents the marked range. (image source: screenshot from LabelImg tool).

(4) Model training: During the model training process, this study selected YOLOv8 as the object detection model. YOLOv8 has the characteristics of lightweight, fast speed, and high accuracy and is particularly suitable for real-time detection tasks. These characteristics make it highly suitable for the rapid identification and detection of gray brick damage to Fuzhou's ancient houses, as demonstrated in this study. In addition, YOLOv8 has

strong capabilities in terms of feature extraction and target positioning and can effectively cope with the complexity and diversity of different types of damage. We divided the training set and the test set in a ratio of 9:1. We used the training set to optimize the model parameters and the test set to verify the model's performance. During the research process, we conducted multiple experiments and made adjustments to the selection of the hyperparameters, focusing on parameters like the learning rate and batch size, to achieve the ideal accuracy and recall level. We adjusted the batch size and learning rate during the training process to prevent the model from overfitting. Simultaneously, we applied data enhancement techniques like flipping, rotation, and color jittering to enhance the model's robustness in various practical scenarios.

(5) Model testing: After the model training was completed, it needed to be tested to evaluate its performance. This study used the test set to evaluate the YOLOv8 model and looked at how well it extracted features of different types of damage at different levels using feature maps. It paid special attention to the cv2 and cv3 modules of the head network in the YOLO model architecture. The purpose of these analyses was to understand the model's ability to extract and express gray brick damage features at different convolutional layers so as to provide a reference for further optimizing it. We primarily observed the model's recognition effect on the gray brick efflorescence and plant growth damage types during the test, as well as any missed or false detections during the detection process.

(6) Model evaluation: This study used multiple indicators to comprehensively evaluate the detection ability of the model, including the precision, recall, F1 score, average precision (AP), and log-average miss rate. Precision measures the accuracy of the model's predictions of damaged instances, while recall gauges the correct identification of all the actual damaged instances. The F1 score is used to balance the trade-off between precision and recall and is an important indicator for comprehensively evaluating model performance. The average precision (AP) is used to measure the comprehensive performance of the model under different confidence thresholds. The log-average miss rate is used to evaluate the effectiveness of the model in reducing missed detections and is particularly suitable for evaluating the model in low-confidence scenarios. This study trained the model for 300 epochs and selected four models for further testing based on the outstanding performance of the above indicators during the training process. We selected the model with the most balanced performance in all aspects as the object of further application.

(7) Model application: After completing the model evaluation, this study applied the model to images taken on site to verify its application effect in actual scenarios. By using unprocessed photos of the gray brick surface of an ancient house in Fuzhou, the model was able to automatically detect and identify two types of damage on the gray brick surface: efflorescence and plant growth. To further verify the accuracy of the model, this study evaluated the field test results and analyzed the model's characteristics and shortcomings as a guide for future research, aiming to continuously optimize the model's performance.

3.4. Model Setup

The YOLOv8 model is used in this study to detect the main types of damage to the gray brick walls of Fuzhou's ancient houses. Since the visual features of gray brick damage are consistent, computer vision models are very suitable for this task. The architecture of the YOLOv8 model consists of three main parts: the backbone, the neck, and the head. Each part has different tasks to ensure that the model can efficiently extract and fuse features to achieve accurate detection of the target (Figure 5). Please refer to Appendix B for the operating environment of the machine learning.

(1) Backbone: The backbone is mainly used to extract features from the input image. In this study, the input is a gray brick image of 512×512 pixels. Multiple layers of convolution operations yield feature maps of various scales, ranging from P1 to P5. The sizes of these feature maps are P1 ($256 \times 256 \times 80$), P2 ($128 \times 128 \times 160$), P3 ($64 \times 64 \times 320$), P4 ($32 \times 32 \times 640$), and P5 ($16 \times 16 \times 640$). These feature maps extract spatial and semantic information from the image layer by layer. The shallower layers (such as P1 and P2) retain

more low-level features, such as edges and textures, while the deeper layers (such as P4 and P5) extract more abstract, high-level features. These features can help the model better identify complex damage types on the gray brick surface.

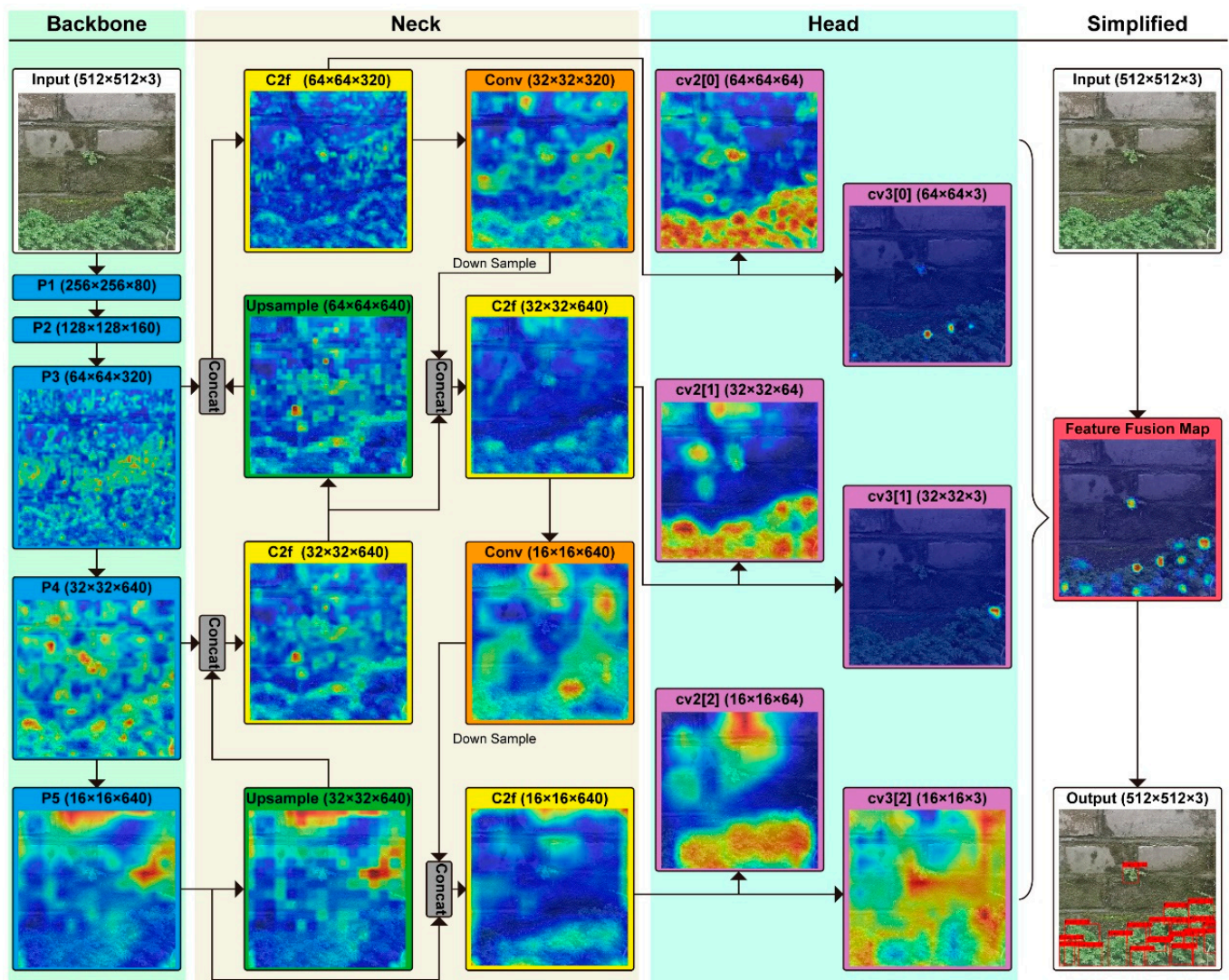


Figure 5. Design of the YOLOv8 architecture used in this study (image source: drawn by the author).

(2) Neck: The role of the neck is to fuse features from different scales so that the model can better handle multi-scale targets. The neck part of YOLOv8 uses a feature pyramid network (FPN) and a path aggregation network (PANet) to fuse features through upsampling and downsampling operations. In this study, the neck part integrates feature maps of various resolutions, ranging from P3 to P5, to enable the model to detect both subtle damage to the gray brick and changes in the overall structure. For example, when the C2f module (for example, $64 \times 64 \times 640$) and the convolution (Conv) module (for example, $32 \times 32 \times 320$) work together, the model can accurately show the efflorescence of gray bricks and the features of plant growth at different sizes.

(3) Head: The head is used for the final target detection and classification. Multiple convolutional layers in the YOLOv8 head generate the final prediction box and classification results. In this study, the cv2 and cv3 modules of the head part are particularly important for extracting gray brick damage features. The feature map size of cv2 is $(64 \times 64 \times 64)$, while the feature map size of cv3 is $(32 \times 32 \times 3)$. By analyzing these feature maps, we can see the model’s ability to recognize different types of damage. For example, the cv2 module extracts relatively medium-scale features, while the cv3 module extracts details

at a smaller scale. These modules work together to ensure that the model can detect both more significant efflorescence phenomena and smaller plant growth areas.

(4) Simplification and fusion: After the feature extraction of the backbone, neck, and head, the multi-scale feature maps are finally fused to generate a feature fusion map, which is used for the final output prediction. In this study, this feature fusion map effectively integrates the feature information of various types of damage on the gray brick surface, helping the model to accurately locate the areas of efflorescence and plant growth. The final output prediction result is a $512 \times 512 \times 3$ image, in which the plant area is marked with red and the efflorescence area is marked with the fluorescent blue.

In summary, the various components of the YOLOv8 model play an important role in gray brick surface damage detection. Specifically, the two main types of gray brick surface damage, namely, efflorescence and plant growth, have different characteristics and complexity. The efflorescence phenomenon usually manifests as more significant regional changes, while plant growth is complex and diverse due to differences in vegetation types and coverage. In the YOLOv8 architecture, the backbone part effectively captures the overall characteristics of efflorescence and the detailed changes in plant growth through feature extraction at different scales. The neck part ensures that the model can focus on both subtle damage to the gray brick surface and damage features in larger areas by fusing feature maps at different scales. The cv2 and cv3 modules in the head part refine and extract features at different scales, allowing the model to accurately identify the significance of efflorescence and the subtle features of plant growth.

4. Field Survey Results: Fuzhou's Ancient Houses (Gu-Cuo) in Fujian Province

4.1. Analysis of Fuzhou's Climate Characteristics

Fuzhou (in older English publications, the name is Romanized as Foochow) is located in the southeastern part of the Chinese Mainland in the Min River estuary area in eastern Fujian [47]. Geographically, Fuzhou is located in a typical estuary basin. Mountains surround the basin, with altitudes typically ranging from 600 to 1000 m [48]. Fuzhou faces northern Taiwan across the Taiwan Strait to the east, Quanzhou City and Putian City to the south, Sanming City to the west, and Nanping City and Ningde City to the north [49]. The terrain is higher in the west and lower in the east. From the Jiufeng Mountain–Daiyun Mountain Range in the west to the Taiwan Strait in the east, the landform types vary from mountains in the central part to low mountains, higher hills, platform plains, and finally the sea [50]. Mountains and hills account for 72.68% of the total area. Fuzhou has an oceanic subtropical monsoon climate, which is warm and humid, with an annual relative humidity of about 77% [51,52]. The annual rainfall in 2007 was 1367.5 mm, and the annual average temperature was 16 to 20 °C (Figure 6). The average annual rainfall in Fuzhou has increased significantly in recent years compared to previous years. This increase has exacerbated the erosion and corrosion effects of rain on gray bricks, necessitating additional maintenance. The average temperature in the coldest months of January and February is 6 to 10 °C, with the average temperature in the hottest months of July and August reaching 24–29 °C (Figure 7). Therefore, the annual average maximum, average minimum, and average temperatures in Fuzhou are tending to fluctuate more over time [53]. That is, in the future, Fuzhou is very likely to have higher summer temperatures and lower winter temperatures, which will lead to a stronger thermal expansion and contraction effect on gray brick and cause greater damage.

However, due to the more significant heat island effect in recent years and the influence of the basin's topography, the temperature at noon in summer is generally as high as over 36 °C [54]. Typhoon weather strongly affects Fuzhou every year. July to September is the typhoon activity period, and the average number of direct typhoon landings per year is two. Due to their underdeveloped technology and limited ability to control the environment, people in the past often had no way to actively control and transform nature and could only try to adapt to it. The enthalpy–humidity diagram shows that, in Fuzhou, comfortable conditions are present for 6.9% of the year (about 602 h). Strong sunlight is present for

15.0% of the year (about 1317 h), requiring shading measures, while an increased internal heat gain is noted for 25.8% of the year (about 2257 h). High air humidity is present for 10.2% of the year (about 895 h), highlighting that indoor dehumidification needs to be strengthened, and for 28.9% of the year (2528 h), the temperature is greater than the human body's tolerance, requiring cooling and dehumidification measures. Low temperatures and humidities are experienced for 18.4% of the year (about 1611 h), and thus indoor heating and humidification need to be strengthened (Figure 8). In Fuzhou, conditions are within a comfortable range for only 6.9% of the time, necessitating year-round sunshade measures. Climate has a profound impact on architectural space. For example, a building's climate environment constrains its architectural form, enclosure structure, structural system, spatial organization, and space layout.

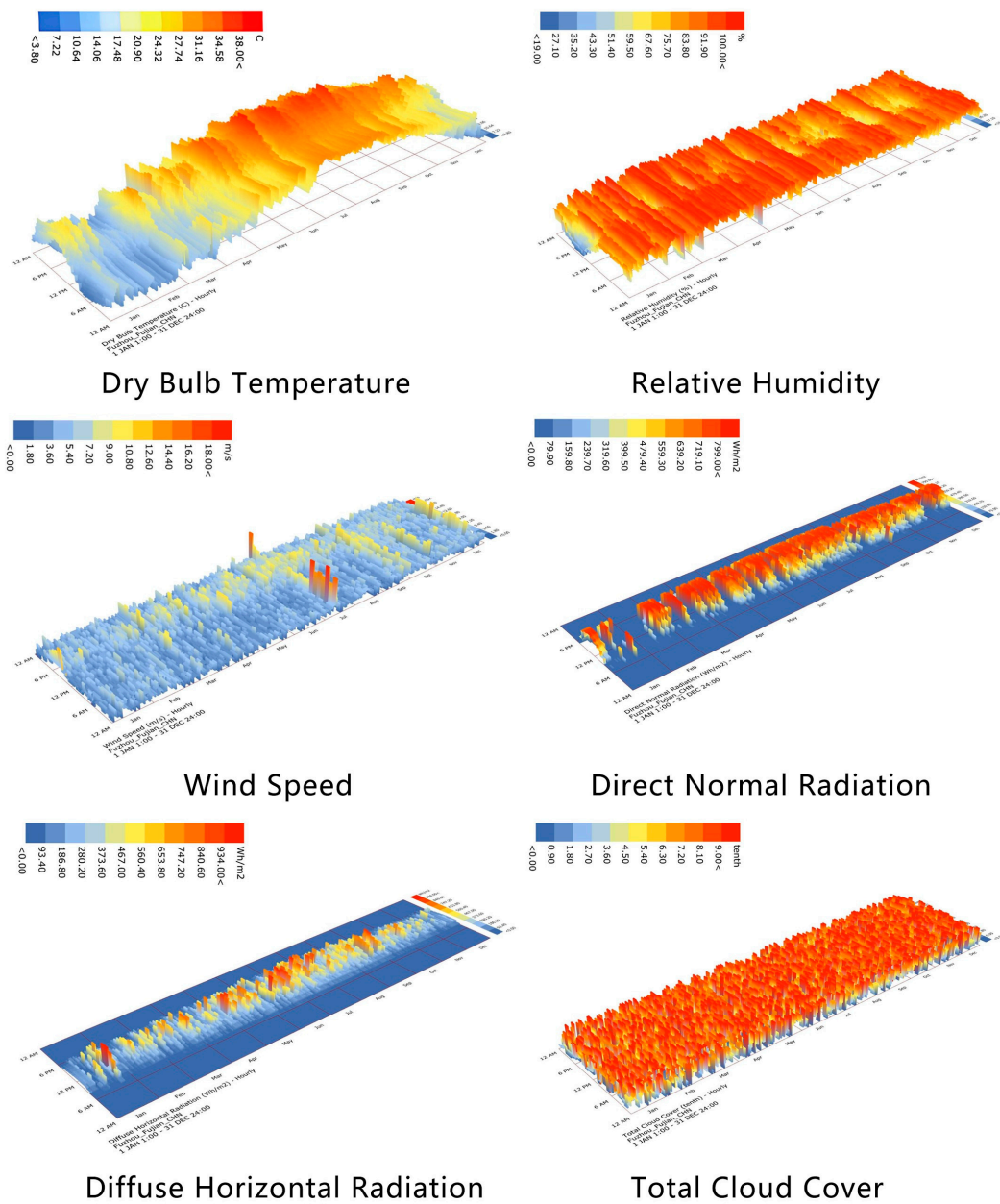


Figure 6. Climate analysis of Fuzhou City (image source: drawn by the author via Ladybug).

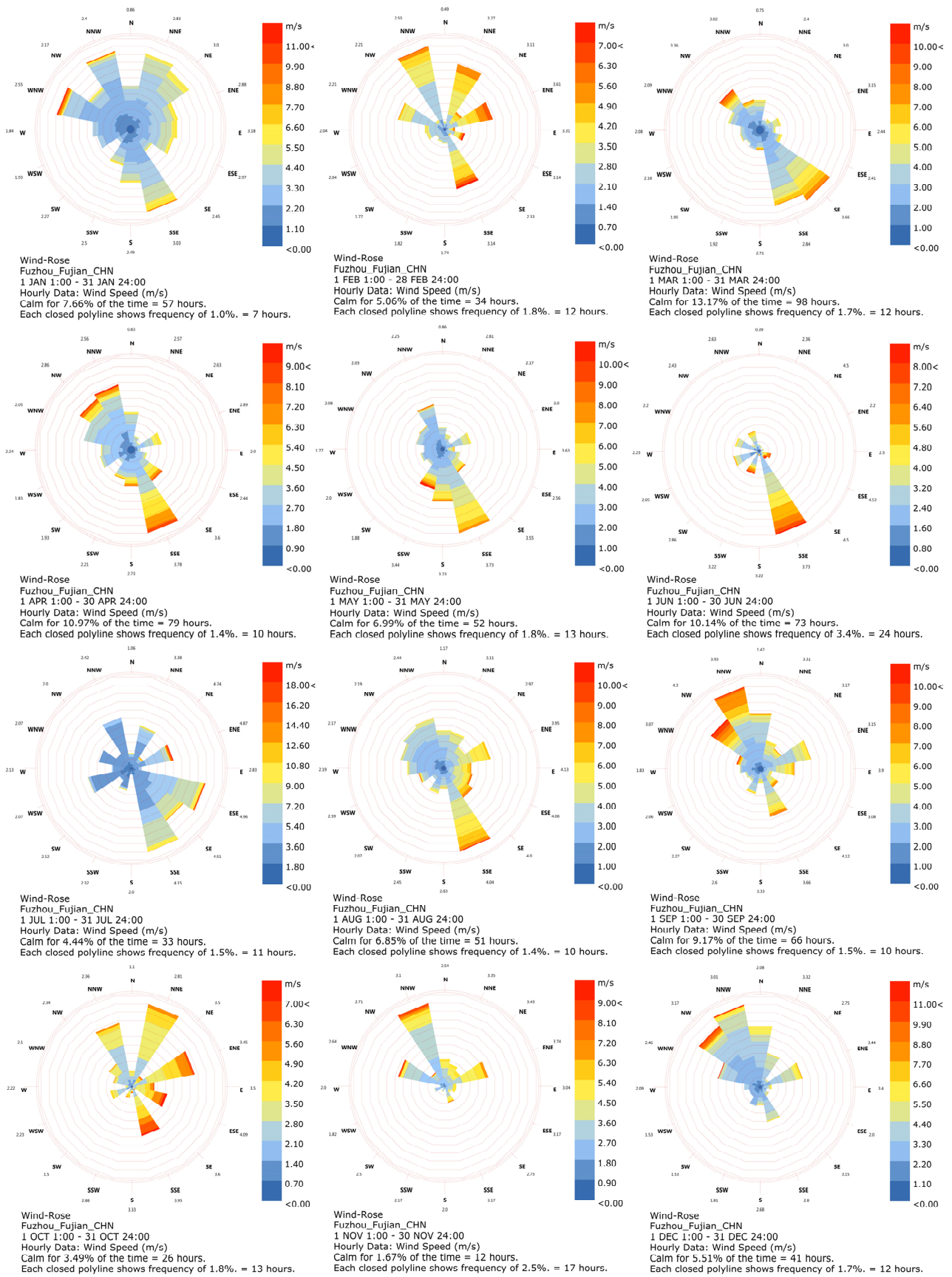


Figure 7. Analysis of the annual wind frequency rise in Fuzhou (image source: drawn by the author via Ladybug).

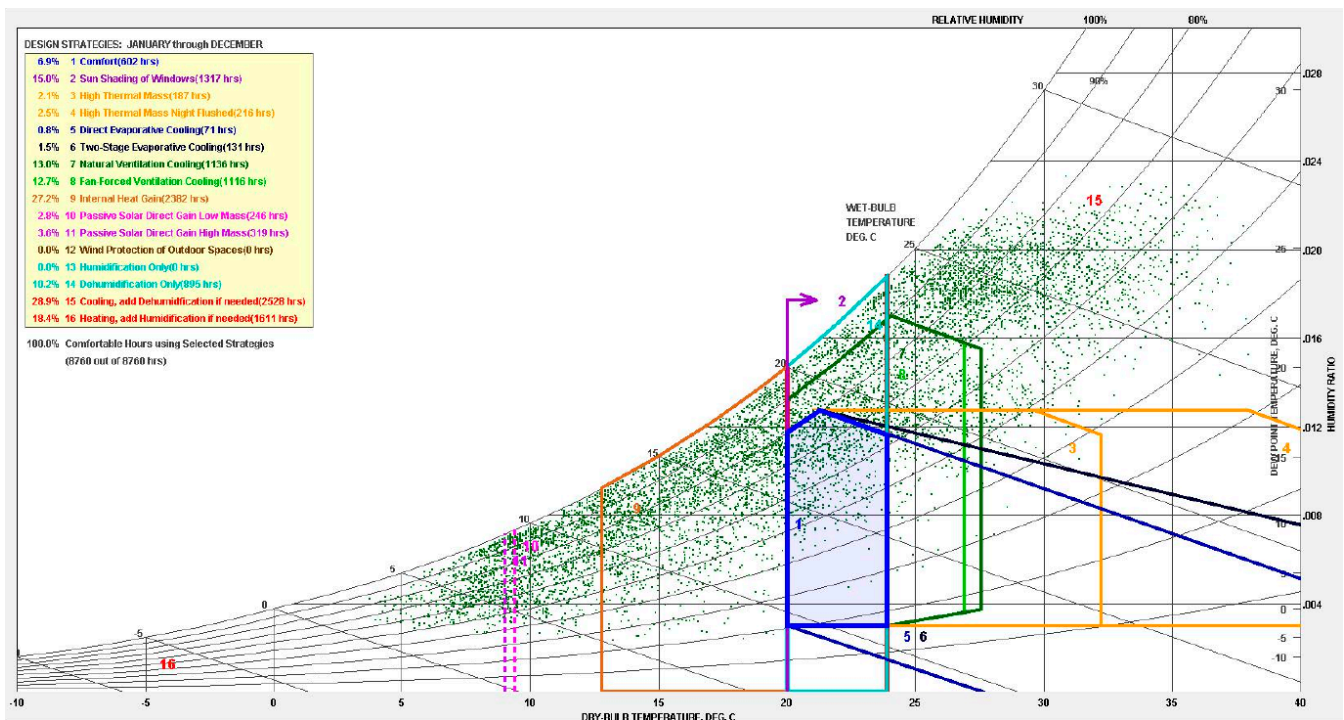


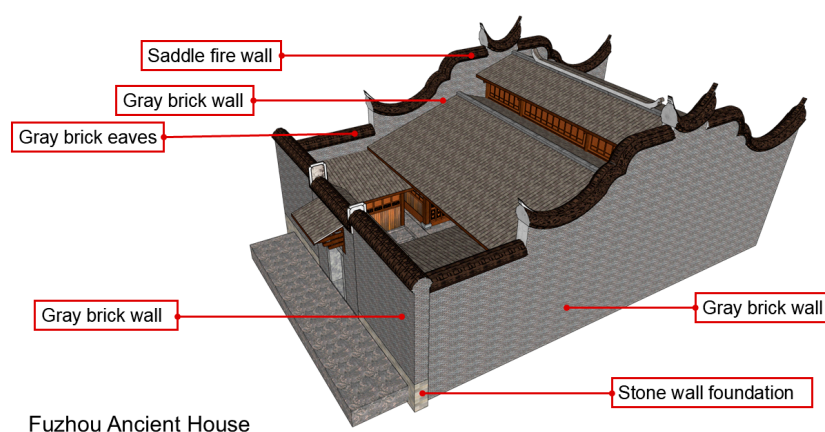
Figure 8. Analysis of the enthalpy–humidity diagram for Fuzhou (image source: drawn by the author via Climate Consultant).

In summary, the design of Fuzhou’s ancient houses prioritizes wind protection and ventilation, waterproof and moisture-proof materials, lighting and sunshade systems, and thermal insulation, among other factors, to adapt to the climate. In order to drain water, houses are usually built with a slope of about 30 degrees, deep eaves, waist eaves on the layered floors, and rain eaves above the windows. All the walls, including the yard walls and fireproof walls, feature tiled slopes, while the gable doors and window openings feature rain eaves. Fuzhou’s high summer humidity, particularly during the rainy season, can reach up to 85%. This high relative humidity makes items susceptible to mildew and condensation that occur on stone surfaces, which can negatively impact their use. In certain buildings, bedrooms are typically constructed on the ground level, while the attic serves as the storage warehouse. The stone column base under the wooden column is also usually used as a moisture-proof feature. Typhoons frequently strike buildings during the summer and autumn seasons, causing significant damage to these structures. To withstand typhoons, builders have constructed single-story buildings on the windward side of the coast, with gables serving as roofs instead of eaves. Some roof tiles are pressed with stones, and the edges are glued with oyster shells. Climate characteristics have affected the architectural form of Fuzhou’s ancient houses, but climate change has further aggravated the surface damage to traditional buildings.

4.2. Wall Brick Construction and Feature Analysis

Fuzhou’s traditional residential architecture has its own system and very distinctive regional characteristics [55]. It belongs to the eastern Fujian residential building style and is characteristic of the Min Chinese-speaking area of the country [56]. This architectural form is largely consistent with the eastern Fujian language spoken in the area. Traditional Fuzhou residential materials primarily consist of wood, with bricks and stones serving as supplements [57]. Their floor plan mostly follows the “three-in-one inner courtyard type”, with the main hall serving as the core. The main hall has three, five, or seven bays, with patios on both sides [58], where this is a verandah. The most notable features of Fuzhou folk houses are the saddle-shaped firewalls, gates, and other structures, which are also unique to Fuzhou and eastern Fujian (Figures 9–14). Fuzhou’s

volcano-sealing wall has a saddle curve shape. The wall stands tall, undulates with the beams, and tilts upward at both ends. It has strong momentum. It is frequently referred to as a saddle wall or horsehead wall; this wall is widely used in China, with the exception of eastern Fujian. The rest of the area is quite bland. The walls are painted with white oyster shell ash or lime, while the tops and corners are adorned with painted sculptures [59]. Some of the sculptures feature a large number of ocean-related elements. Furthermore, to withstand typhoons, the majority of houses on the seaside or islands in Fuzhou are constructed from stone and feature stone tiles [60]. Fuzhou is filled with traditional residential buildings, some of which are highly representative. Fuzhou's historical and cultural districts still retain many former residences of celebrities. These historical buildings have experienced changes and have suffered varying degrees of damage. Fortunately, society's increasing attention toward historical heritage has led to the restoration of these former residences in recent years. At historical building restoration construction sites, many bricks removed from old buildings have been found [7]. The bricks exhibit a distinctive blue-gray color, are concave on both sides, and prominently bear the words "Fu Shou" [61]. Researchers have discovered large quantities of this gray brick in the Three Lanes and Seven Alleys Historic District of Fuzhou's center, which is historically the residential area of Fuzhou's wealthy families. It covers an area of 40.2 hectares and has 268 ancient Ming and Qing dwellings. It is China's largest and most complete collection of ancient Ming and Qing buildings preserved in urban centers [62]. The entire Three Lanes and Seven Alleys Historic District is listed as a key national cultural relic protection area in the "Museum of Ancient Architecture of the Ming and Qing Dynasties".



Fuzhou Ancient House

Figure 9. The location of gray brick in an ancient Fuzhou house (image source: drawn by the author).

Fuzhou has a long history of using bricks. In 1956, tomb bricks excavated from ancient tombs in Xindian, Wenlinshan, and other places were identified as products of the Han and Jin Dynasties. In the second year of Shunzhi in the Qing Dynasty (1645), Wu Xiangtai, a native of Wufeng Village, Gaogaishan, Min County, built a kiln in the shape of a horseshoe, making blanks from clay, and used Miscanthus as a fuel to burn them into bricks. By adding water to cool the bricks during the firing process, they became blue-gray, hard in texture, and crisp in sound, hence the name "gray brick" [7]. Afterwards, villagers in Yixu, Zhulan, Pukou, and other places built kilns to imitate them and passed them down from generation to generation. Therefore, bricks occupy an important position in Fujian's architectural culture and are the key to distinguishing the characteristics of architectural culture. Mr. Huang Hanmin wrote the following in his book *Old Houses: Fujian Folk Houses*: Since ancient times, the brick walls of traditional Chinese buildings have been built with gray bricks, and the folk houses in various provinces on the mainland also use gray bricks. Only Fujian has used red bricks to build houses; Taiwan's traditional red brick buildings also originated in Fujian. Therefore, the division into "red brick area" and "gray brick area" can more clearly reflect the appearance of traditional Fujian dwellings. Quanzhou is the center of the "red brick cultural area", while Fuzhou is the center of the "gray brick cultural area" [63]. Both red and gray bricks are made of clay fired at high temperatures, and the difference in color lies in the different firing processes. Whether they are red or gray bricks, the unique masonry techniques used to make them and the construction

culture reflect the natural and cultural environment of Fujian. The gradual loss of traditional craftsmanship and the damage to the brick wall surfaces of these traditional buildings urgently require attention—traditional buildings require protection.

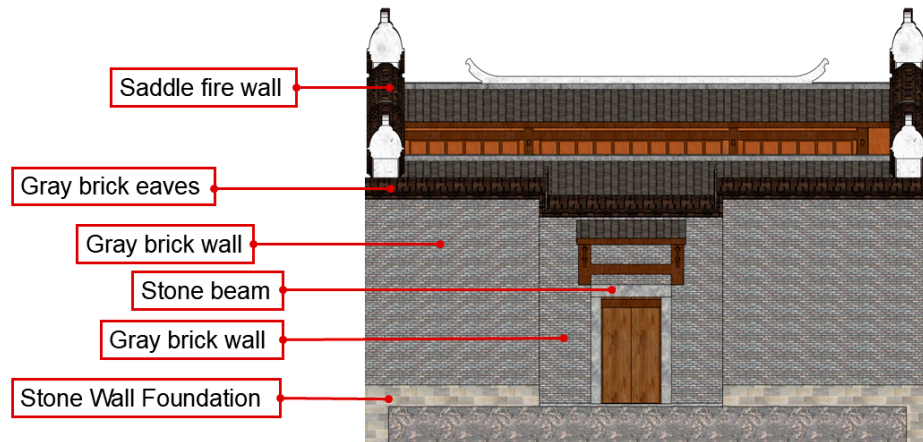


Figure 10. Ancient houses in Fuzhou feature gray brick on their façade (image source: drawn by the author).

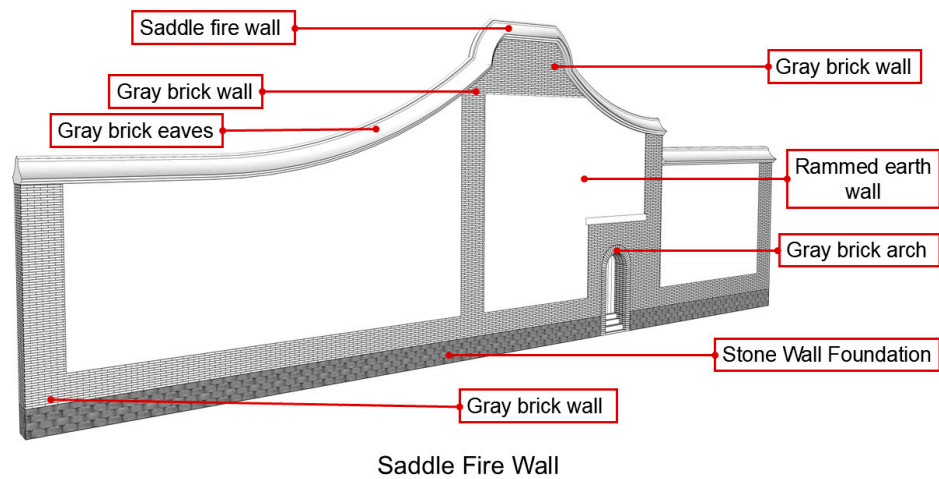


Figure 11. The location of gray bricks in the saddle fire wall (image source: drawn by the author).

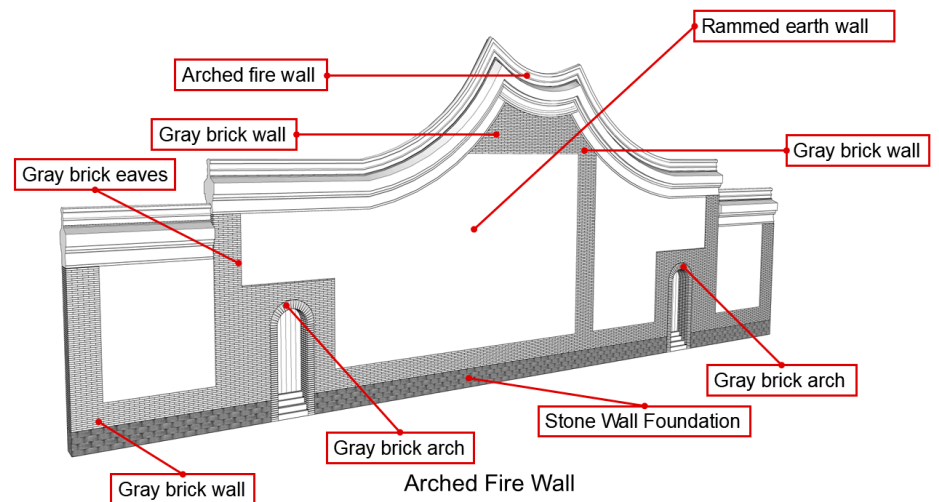


Figure 12. The location of gray bricks in the arched fire wall (image source: drawn by the author).

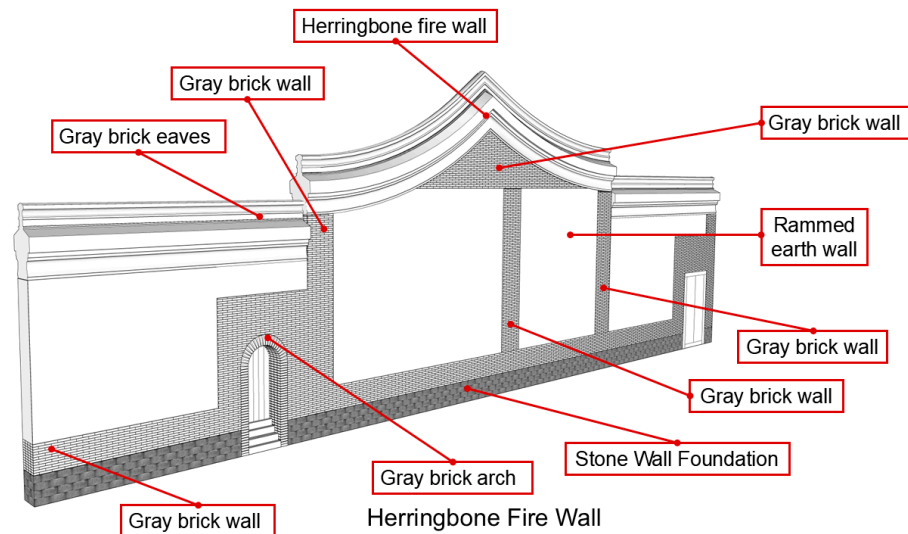


Figure 13. The location of gray bricks in the herringbone fire wall (image source: drawn by the author).

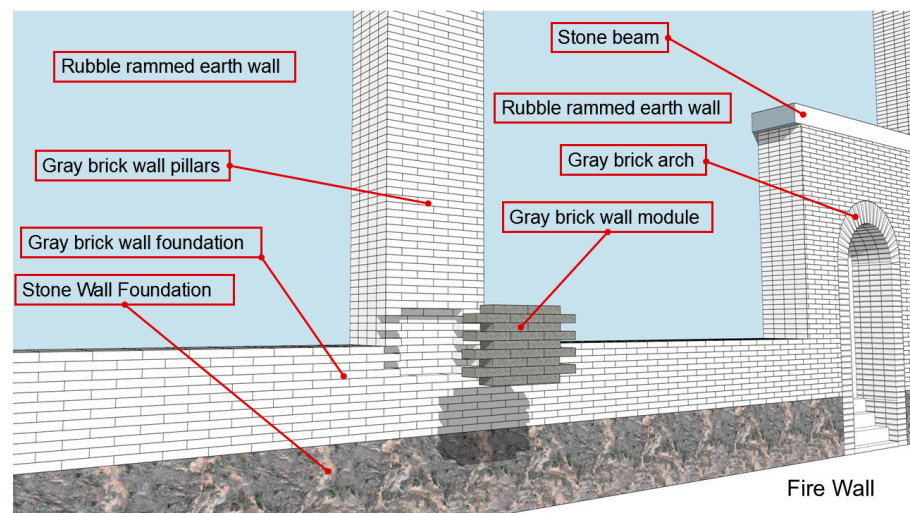


Figure 14. The distribution of gray bricks in the walls of Western-style buildings (image source: drawn by the author).

4.3. Analysis of Damage Types and Factors in Wall Bricks

Fuzhou is located on the outer belt of the southeast coastal seismic belt and belongs to the Pacific Rim seismic belt [64]. Similar to Taiwan, it is an earthquake-prone area, characterized by a shallow focal depth, for which strong tremors on the surface are common. Since 2000, Fuzhou and neighboring cities have experienced more than 40 small earthquakes, with a very high frequency. The gray brick buildings of ancient houses are affected by geological structures and are prone to cracking. These buildings are vulnerable to collapse and damage from repairs. The summer on the southeast coast is a season of heavy rainfall and frequent typhoons [65]. The destruction of ancient gray brick buildings is primarily caused by the high temperature and high humidity environment. Long-term accumulation of groundwater causes moisture to rise through capillary action, damaging the surface of the gray bricks. Table 1 shows the relevant statistics found by researchers in this investigation concerning the damage types of gray brick buildings in ancient houses in Fuzhou.

Table 1. Investigation of the damage types of gray brick buildings in ancient houses in Fuzhou.








Type	Damage Location	Cause	Damage Degree	Image
White bloom (efflorescence) phenomenon	Gray brick corners, stone wall foundations or other parts	Soluble salts are contained in bricks, mortar joints, and stone materials. Water, through capillary action, precipitates calcium hydroxide, alkaline metal ions, etc., on to the surface of the bricks, leaving white marks after drying.	☆☆☆☆☆	
Crystalline salt	Stone wall foundations, gray brick floors, gray brick walls	Water containing mineral salts penetrates into the bricks through the surface or outside. When the water is precipitated on the wall surface, it produces white crystals after drying.	☆	
Moss growth, local mold	Stone wall foundations, gray brick floors, gray brick walls (interior walls)	Groundwater, long-term ground puddles, or sewage in drainage pipes invade bricks or mortar joints through capillary action, causing moisture to rise and promote moss growth; the roof is leaking, rainwater flows along the wall, and mold appears.	☆☆☆	
Weathering corrosion	Gray bricks, mortar joints	Rainwater intrusion, typhoons, and salt erosion.	☆☆	
Brick surface delamination	Gray bricks	Weathering, painting, using overly hard plaster, or excessive cleaning cause damage, accelerate the deterioration of the brick surface, and lead to delamination.	☆☆☆	
Cracks	Gray bricks	There are fine cracks in the brick itself, and long-term temperature changes, rain erosion, and thermal expansion and contraction cause the cracks to become larger.	☆☆☆	
Wall cracks	Gray bricks	Earthquakes, overload bearing, foundation sinking, etc., change the strength of the brick structure, resulting in longer cracks.	☆☆☆☆	

Table 1. Cont.

Type	Damage Location	Cause	Damage Degree	Image
Wall peeling	Gray brick walls	Surface natural weathering, external force impact.	☆☆☆	
Mortar joint erosion	Gray brick walls	Weathering erosion.	☆☆☆	
Plant invasion	Gray brick mortar joints	Tree root expansion and growth, shrubs, herbs, vines, and epiphytes.	☆☆☆☆☆	
Human damage	Roof tile surface, gray brick walls, stone wall foundations, building interiors, gray brick floors	Water and electricity pipelines, pencils, chalk, signature pens, spray paint graffiti, smoke, planting crops, theft, etc.	☆☆	
Improper repair	Stone wall foundations, gray brick walls	Modern cement mortar directly cover the wall, causing irreversible damage.	☆☆☆	

Source: The authors' statistics based on the field survey results. The number of ☆s indicates the severity of the surface damage.

After investigation, the researchers found that while there are many types of damage to the surface of gray bricks, some are of low severity. Therefore, the researchers selected the two most common and concerning types of surface damage for a detailed summary and subsequent label creation. After field surveys and image collection analysis, the researchers classified the damage into two main types: efflorescence and invasive plant growth. Figure 15 below shows the two most evident types of surface damage to gray brick and the collection size of the subsequent labeling samples.

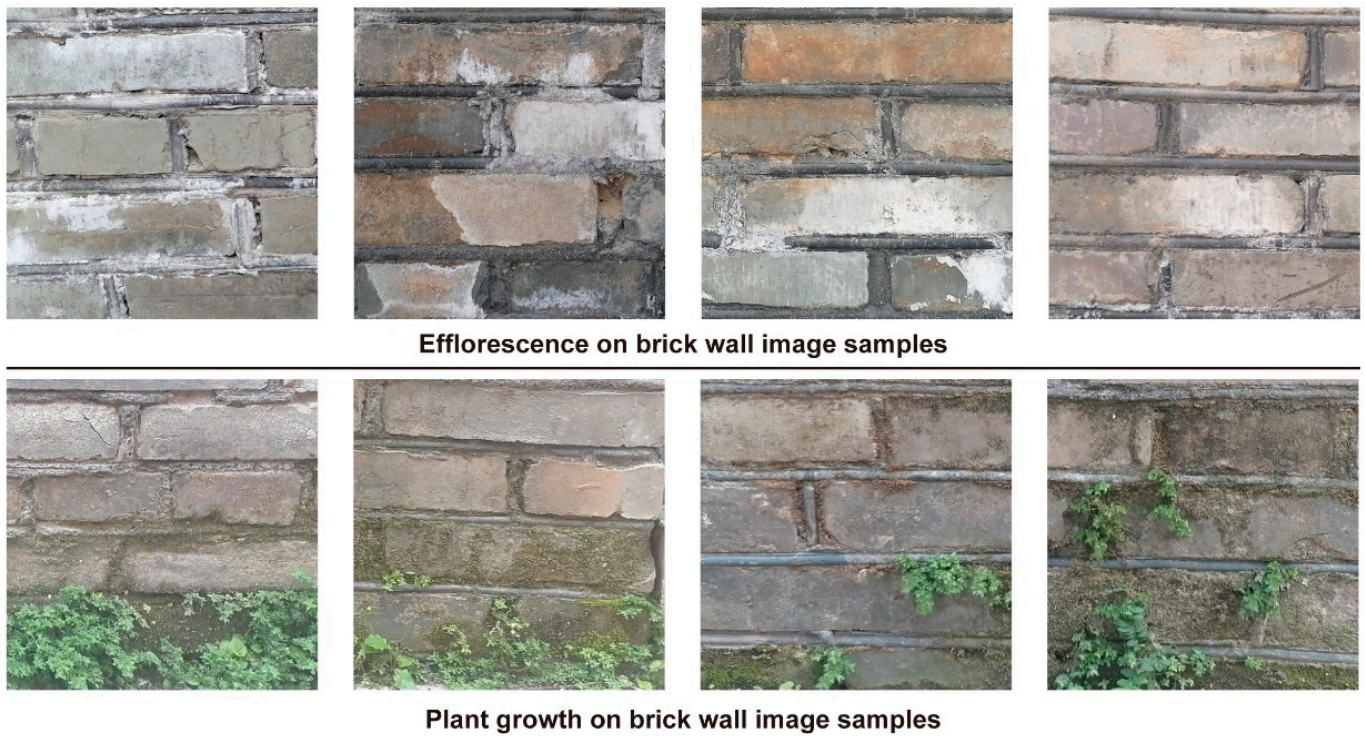


Figure 15. Schemes follow the same formatting, all images are normalized to 512×512 pixels. (image source: drawn by the author).

5. Automatically Identify Model Construction Results

5.1. Model Optimization Experiments

In order to improve the accuracy and recall rate of the model, we conducted 10 experiments in total. We continuously optimized and adjusted the hyperparameters to select the model configuration most suitable for gray brick wall damage detection in relation to Fuzhou’s ancient houses. Figure 16 displays the specific experimental results.

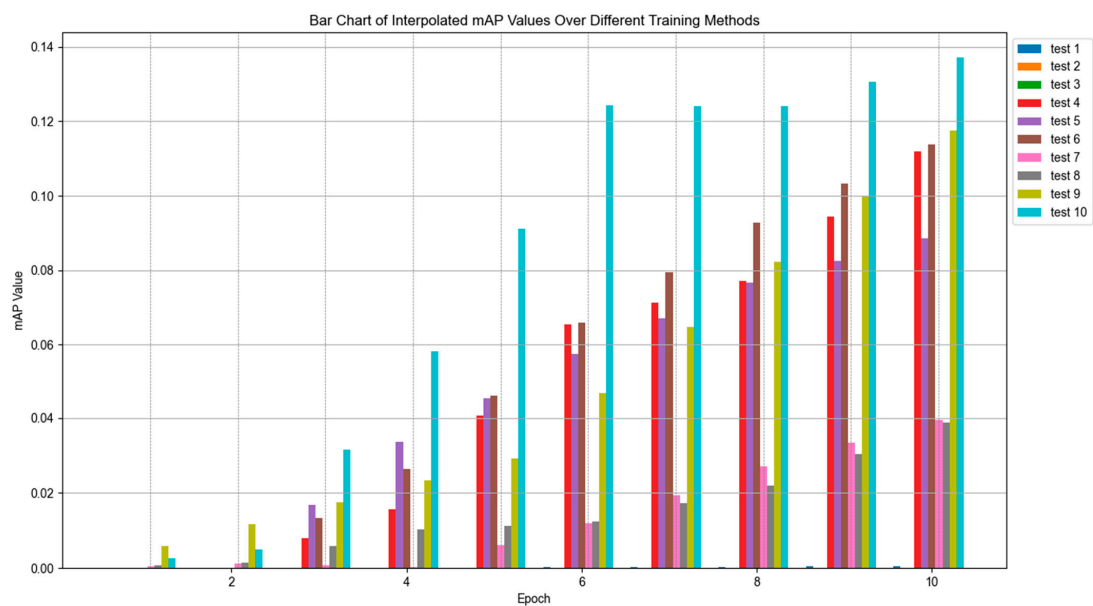


Figure 16. The mAP numerical statistics of the first ten epochs of ten model optimization experiments (image source: drawn by the author).

(1) In the first experiment, we enabled data augmentation and adjusted the training batches to 32 and 16 (before freezing and after thawing), but the results showed that the model's mAP was almost zero. This indicates that the parameter settings of the data augmentation were too complex, resulting in the model being unable to effectively learn features. As long as the features of gray brick efflorescence and plant growth stay mostly the same, complex data augmentation might make it difficult for the model to accurately identify useful features.

(2) In the second experiment, the training batches were reduced to 16 and 8, and the number of training images was increased to 150. The second experiment only slightly improved the mAP value to 0.000002. Compared to the first experiment, the reduction in batches alleviated some of the training pressure on the model, but complex image augmentation still disturbed the characteristics of efflorescence and plant growth, making the improvement less obvious.

(3) In the third experiment, this study decreased the values of each data enhancement to minimize the impact of unnecessary image transformation on the model, resulting in an increase in the mean average precision (mAP) to 0.000045. This demonstrates that reducing the magnitude of the data enhancement can enhance the model's focus on the target features, particularly in the extraction of detailed features related to gray brick surface damage.

(4) In the fourth experiment, only mosaic enhancement in terms of the data enhancement was turned on, and the mAP increased to 0.015723. Mosaic enhancement effectively increased the diversity of the training data, particularly by providing more samples from different manifestations of efflorescence and plant growth, which, in turn, improved the model's ability to generalize features.

(5) In the fifth experiment, we turned off all the data enhancements, leading to a further increase in the mAP to 0.033756. This shows that when the sample size is limited, turning off the data enhancement can reduce unnecessary image change interference and allow the model to focus more on the damaged features of the gray brick surface, which is particularly effective for extracting stable visual features.

(6) In the sixth experiment, we increased the training samples to 250, resulting in an increase in the mAP to 0.026465. Although increasing the sample size generally helps improve the model performance, increasing the sample size did not significantly improve the model performance due to the relatively simple features of efflorescence and plant growth.

(7) In the seventh experiment, the training samples were further increased to 300, but the mAP dropped to 0.000228. This could potentially be attributed to the inconsistent sample annotation, which resulted in an increase in annotation errors during model training, particularly in the areas of coverage and morphological diversity of plant growth. The inaccuracy of the annotation significantly affected the performance of the model.

(8) In the eighth experiment, we streamlined the training samples to 100 and increased the mAP to 0.010190. Reducing the sample size while improving the annotation quality verified the impact of annotation errors on the model performance when the sample size is large, especially in terms of the more complex targets such as efflorescence and plant growth.

(9) In the ninth experiment, we used model-assisted annotation to enhance the quality of the samples' annotations. We reduced the training samples to 49 and significantly improved the mAP to 0.058166. This shows that high-quality annotation is more important than quantity. Model-assisted annotation can effectively reduce human errors, thereby enhancing the model's ability to identify the type of surface damage on gray bricks.

(10) The tenth experiment was the most successful one. We set the hyperparameters of the model as follows: we adjusted the batch size to 4 and 2 (before freezing and after thawing), reduced the learning rate `Init_lr` to $1e-2$, set the `Min_lr` to 0.01 of the `Init_lr`, set the optimizer type to SGD, set the internal parameter momentum of the optimizer to 0.937, set the `weight_decay` to 5×10^{-4} , and used the cosine learning rate reduction method.

The mAP of the final trained model exceeded 0.5, which shows that after adjusting the hyperparameters and optimizer, the model showed a good mAP in relation to the two types of damage recognition, namely, efflorescence and plant growth, and reached a level that can be further experimented with and applied.

Through these 10 experiments, this study summarizes the most suitable hyperparameter settings for training the gray brick wall surface damage detection model of Fuzhou's ancient houses. This is achieved by ensuring the quality of the sample annotation, reasonably controlling the batch size and learning rate, and minimizing or avoiding data enhancement methods. The experimental results indicate that given the relatively consistent efflorescence of gray bricks and the characteristics of plant growth, complex data enhancement may hinder the model's ability to focus on the target features, thereby reducing the detection accuracy. To improve the model's ability to detect things accurately and reliably, it would be better to focus on high-quality data annotation and train it by carefully controlling the number of samples.

5.2. Loss During Model Training

Figure 17 displays the changes in the training loss, validation loss, and mean average precision (mAP) during model training in this study. During the entire 300-epoch training process, it can be seen that the training loss and validation loss exhibit a clear downward trend in the first few epochs, which means that the model quickly learned the characteristics of the damaged gray bricks in the initial training stage. In the first epoch, the maximum value of the training loss is 157.42, and the maximum value of the validation loss is 130.76. As the training progresses, the training loss and validation loss gradually decrease. In the 23rd epoch, the validation loss reaches a minimum of 5.40, which shows that the model fits the validation set well at this time and overfitting has not yet occurred.

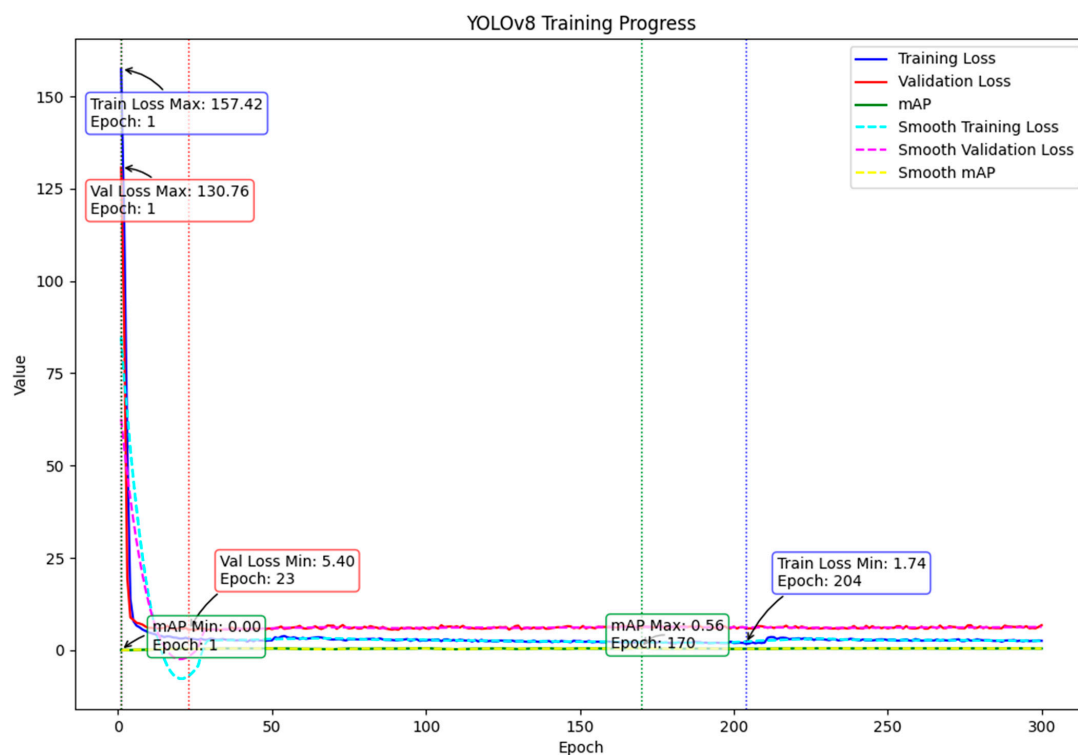


Figure 17. Loss value change trend during model training (image source: drawn by the author).

The training loss reaches a minimum of 1.74 at the 204th epoch of training, which indicates that the model fits the training set very well at this time. Generally speaking, a decrease in training loss means that the model is constantly improving its adaptability to the input data. However, too little training loss may also mean that the model overfits the

training data and loses the ability to generalize to unknown data. Therefore, although the training loss has reached the minimum value, the validation loss has not continued to decrease significantly but has remained at a relatively stable level. The model's generalization ability needs more consideration.

The change in the mean average precision (mAP) is an important indicator to measure the detection ability of the model throughout the training process. Figure 17 shows that the initial model cannot accurately detect the damage type of gray bricks, as the mAP is 0 at the first epoch. As the training progresses, the mAP gradually increases and reaches a maximum value of 0.56 at the 170th epoch, indicating that the model has achieved the best detection ability for gray brick surface efflorescence and plant growth at this stage. The increase in the mAP shows that the model is constantly learning and optimizing the ability of feature extraction and classification, especially in identifying gray brick efflorescence and plant growth. The two types of damage show excellent accuracy.

Figure 17 also shows that the training loss, validation loss, and mAP are essentially stable in the later stages of training, indicating that the model's learning has reached saturation and no significant improvement has occurred. This study selected the model with the smallest validation loss at the 23rd epoch, the model with the largest mAP value at the 170th epoch, the model with the smallest training loss at the 204th epoch, and the model trained at the end of the 300th epoch for further testing and application. These models represent the best performance at different training stages, including the fitting effect of the training set, the accuracy of the validation set, and the overall detection accuracy.

In summary, the changing trends of the loss and mAP in the model training reflect the model's rapid learning in the early stage, feature extraction optimization in the middle stage, and stable training in the later stage. The minimum value of the validation loss and the maximum value of the mAP correspond to the optimal state of the model in terms of the generalization ability and detection accuracy, while the minimum value of the training loss reflects the model's full learning of the training data.

5.3. Model Testing Indicators

The researchers analyzed and compared the detailed test results of the four models selected above, as shown in Figure 18. We analyzed the test results of the 23rd, 170th, 204th, and 300th epoch models and found that different models performed differently in terms of different indicators. Among them, the 170th epoch model performed regarding overall performance, with the average precision (AP) of the gray brick efflorescence detection reaching 0.90, an F1 score of 0.77, and a recall rate of 0.62. The model performed relatively well in plant growth and gray brick efflorescence damage detection. This shows that the model has achieved a good level of feature extraction and classification and has high detection accuracy and stability.

In contrast, the 23rd epoch model performed poorly, exhibiting low average precision, particularly for the gray brick efflorescence and plant growth damage types, with recall rates of just 0.02 and 0.12, respectively. This may be due to the failure of the model to fully learn complex features in the early stage, resulting in insufficient recognition of smaller damaged areas and different types of features in the image.

Although the 204th epoch model performed best in terms of the training loss, its average precision and F1 score were still low, especially for the plant growth types, with an average precision of 0.32 and a recall of 0.26. The low recall rate indicates that the model missed many detections during the detection process, which may be due to overfitting resulting in insufficient generalization ability on the validation set.

The 300th epoch model, as the final trained model, performed stably but failed to surpass the 170th epoch model. The average precision was relatively consistent, but it was still slightly inferior to the 170th epoch model in terms of the recall and F1 score. This shows that in the later training, the model has become saturated and failed to significantly improve its detection performance.

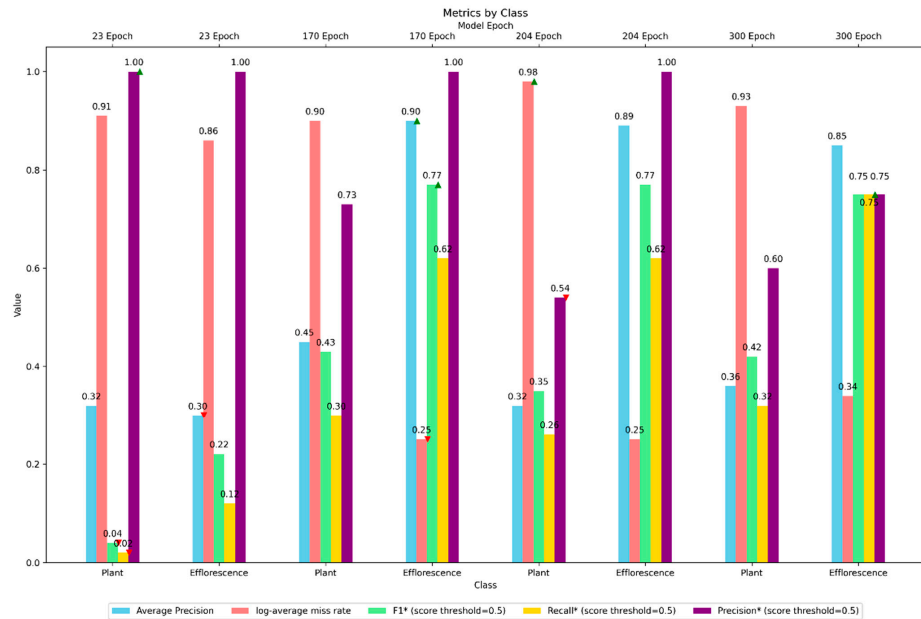


Figure 18. Performance statistics of the models at different epochs. (asterisk * in the figure indicates the median). In the figure, F1* indicates score threshold = 0.5; Recall* indicates score threshold = 0.5; Precision* indicates score threshold = 0.5. (image source: drawn by the author).

In summary, the 170th epoch model performed best in relation to all the indicators, especially in terms of the average precision and recall, showing excellent detection and generalization capabilities. Therefore, this study uses the 170th epoch model as the optimal choice for the subsequent practical scenario testing and application. The 23rd epoch model and the 204th epoch model exhibited distinct defects during the early training stage, primarily manifested in the model’s low recall rate and overfitting.

Figures 19–22 show the confusion matrix of the above four models for detailed analysis. The confusion matrix is used to intuitively display the prediction accuracy of the model for different categories, especially the classification effect and error type of the model in each category.

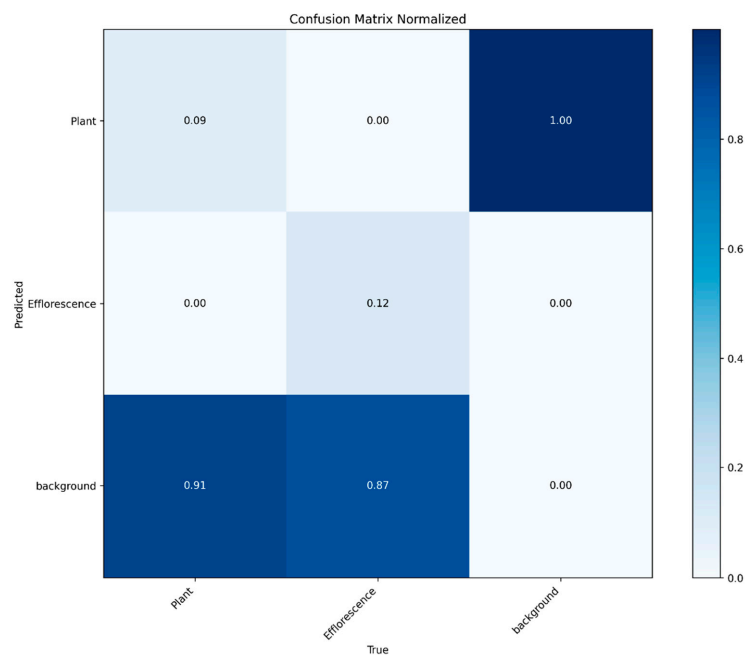


Figure 19. Confusion matrix of the 23rd epoch model (image source: drawn by the author).

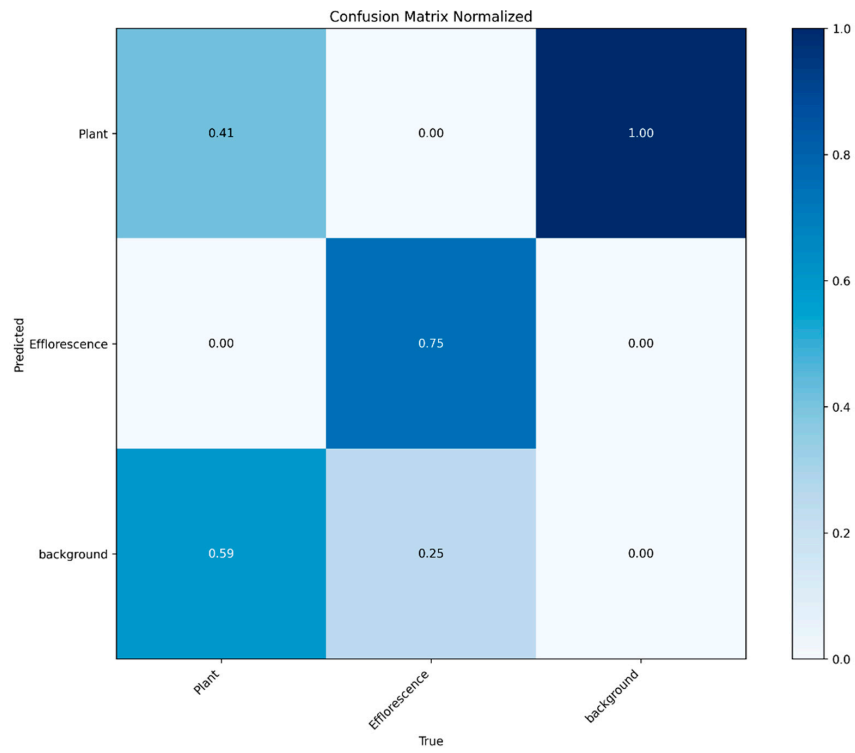


Figure 20. Confusion matrix of the 170th epoch model (image source: drawn by the author).

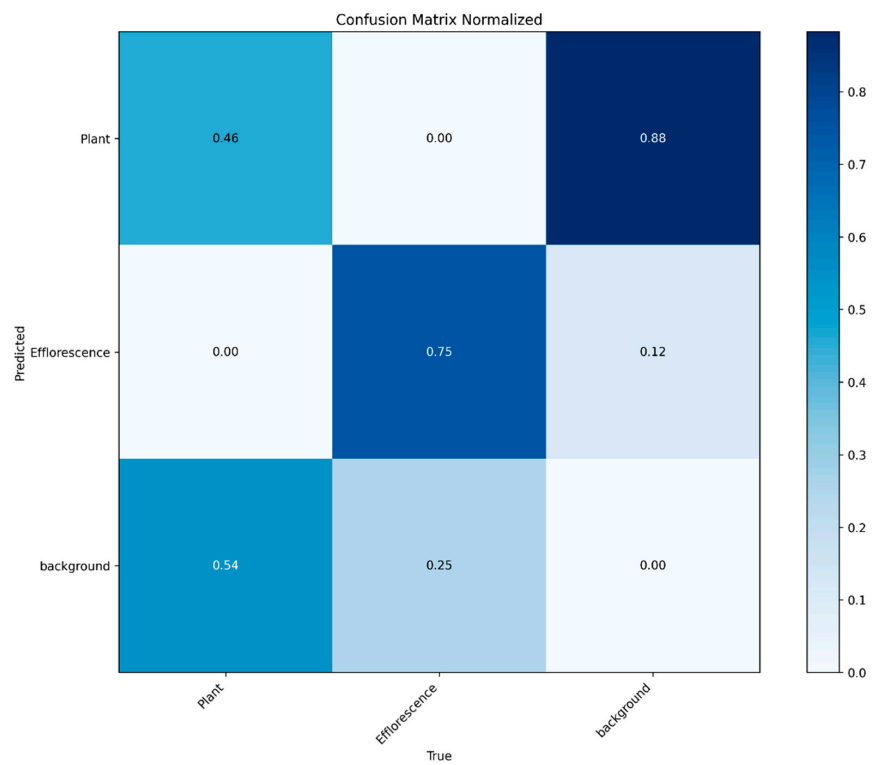


Figure 21. Confusion matrix of the 204th epoch model (image source: drawn by the author).

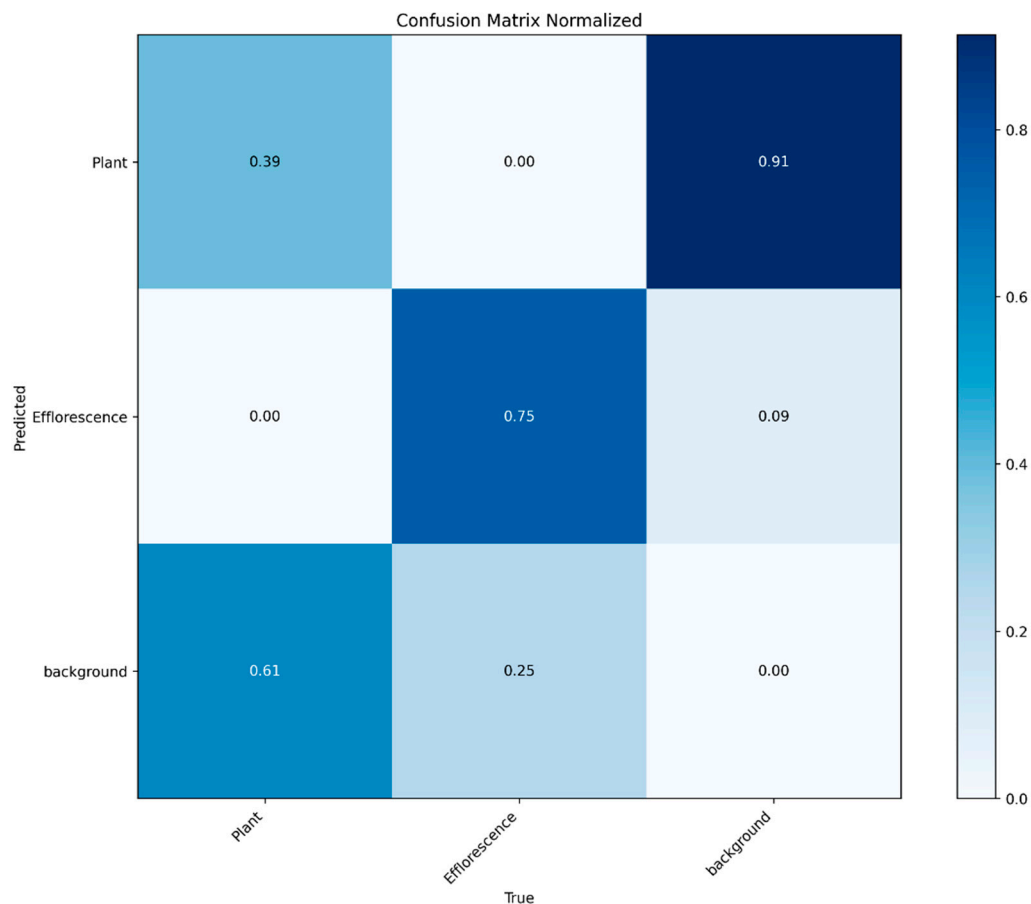


Figure 22. Confusion matrix of the 300th epoch model (image source: drawn by the author).

Figure 19 shows the confusion matrix of the 23rd epoch model, reflecting its classification performance between different damage types (plant growth, gray brick efflorescence, and background). The color depth and numerical values in the matrix represent the correct recognition rate and misclassification rate between different categories. The specific analysis is as follows.

(1) Plant growth category: The model only correctly identified 9% of the plant growth samples, while 91% were mistakenly classified as the background category, showing a significant false detection problem. This shows that the model has a large deficiency in identifying plant growth features, and its feature extraction ability is weak, making it difficult to effectively distinguish plant growth from the background.

(2) Gray brick efflorescence category: In the detection of gray brick efflorescence, the model performed slightly better, with a correct recognition rate of 12%, and was not misclassifying as other damage types. However, the model mistakenly classified 87% of the gray brick efflorescence samples as the background category, indicating its difficulty in distinguishing gray brick efflorescence from background features. This may be because the color or texture of gray brick efflorescence is similar to the background in some cases, causing model confusion.

(3) Background category: There are also obvious errors in the prediction of background samples. The model tends to misclassify plant growth and gray brick efflorescence as background categories, especially in efflorescence samples, where the misclassification rate is as high as 87%. This large number of false positives indicates that the model fails to effectively extract and distinguish damage features when dealing with non-damaged areas, resulting in the low classification accuracy of background samples.

Overall, the 23rd epoch model did not perform well in identifying the plant growth and gray brick efflorescence damage types, particularly due to the high false positive rate

of plant growth categories and serious confusion of background categories. The feature extraction and classification capabilities of the model have not been fully optimized, and more training may be needed to improve the recognition effect of different damage features and enhance the sensitivity to subtle differences.

Figure 20 shows the confusion matrix of the 170th epoch model, from which it can be seen that the model's classification performance between different damage types has improved. The following is a detailed analysis of the different categories.

(1) Plant growth category: The model correctly identified 41% of the plant growth category, which is a significant increase from the 9% of the 23rd generation model. However, 59% of the plant growth samples were still incorrectly classified as background. This shows that after more training, the model's ability to recognize plant growth features has improved, but it is still difficult to completely distinguish between plant growth and background features.

(2) Gray brick efflorescence category: In the recognition of gray brick efflorescence, the model performed well, with a correct recognition rate of 75% and no misclassification as other damage types. This shows that the model has extracted alkali features more fully and can stably identify such samples, indicating that it has successfully learned the key features of gray brick efflorescence during training.

(3) Background category: There is still a problem of false detection in the prediction of background samples, especially in gray brick efflorescence samples; 25% of the efflorescence samples were incorrectly classified as background. This may be because the color or texture features of gray brick efflorescence are similar to the background in some cases, making it difficult for the model to distinguish correctly.

The overall performance of the 170th epoch model significantly improved compared to the 23rd epoch model, especially in the plant growth category, where the recognition rate increased by 32%. This shows that by increasing the number of training times and optimizing the model structure, the model's feature extraction ability and classification performance have been effectively improved. However, the confusion problem between different damage types and the background still exists, which may be related to the certain visual similarity of these features, resulting in the model still facing challenges in distinguishing between them.

Figure 21 shows the confusion matrix of the 204th epoch model, reflecting the model's classification between the plant growth, gray brick efflorescence, and background categories. The following is a detailed analysis of different categories.

(1) Plant growth category: The 204th generation model has a correct recognition rate of 46% for the plant growth category, which is an improvement over the 41% of the 170th epoch model. However, 54% of the plant growth samples are still misclassified as background, indicating that the model still has difficulty distinguishing plant growth from background features. Although the model has improved in terms of feature extraction, the similarity between plant growth and background still leads to a high confusion rate.

(2) Gray brick efflorescence category: For the gray brick efflorescence category, the model's correct recognition rate remains at 75%, which is consistent with the 170th epoch model, but 12% of the efflorescence samples are misclassified as background. The model shows a certain stability in the detection of efflorescence samples, but the features of some samples are similar to the background, resulting in misclassification. This similarity may be due to the similarity in color and texture between alkali and background under certain lighting conditions.

(3) Background category: In the background category, the model misclassified 25% of the efflorescence samples and 12% of the plant growth samples as background, which shows that the model has difficulty in effectively distinguishing damaged and undamaged areas in some cases, especially when the features are close. Since the color or texture of gray brick efflorescence and plant growth partially overlaps with the background, the model produced more false positives on these samples.

Overall, the 204th epoch model has improved in the detection of the plant growth category compared with the 170th epoch model, but the confusion between the background

category and other damage categories is still obvious, especially when the features are similar. It is more likely to be misjudged. This suggests that we may need to further optimize the model in the future to reduce the confusion between the background and the other categories and improve its recognition accuracy in complex scenes.

Figure 22 shows the confusion matrix of the 300th epoch model, reflecting the classification performance of the model between the plant growth, gray brick efflorescence, and background categories. The following is a specific analysis of different categories.

(1) Plant growth category: The correct recognition rate of the 300th epoch model on the plant growth category is 39%, which is lower than that of the 204th epoch model. At the same time, 61% of the plant growth samples are misclassified as background. This indicates that the generalization ability of the model may be weakened in the later stage of training, and a slight overfitting occurs, resulting in a decrease in its detection effect on the plant growth category.

(2) Gray brick alkali category: For the gray brick efflorescence category, the model performance is relatively stable, with a correct recognition rate of 75%, which is consistent with the 204th epoch model, and 9% of the efflorescence samples are misclassified as background. This shows that the model maintains high stability in the extraction of gray brick efflorescence features and can effectively identify efflorescence samples, but due to some similar features of efflorescence and background, there are still a small number of misclassifications.

(3) Background category: There is still significant confusion in the classification of the background category, with 25% of the efflorescence samples and a large number of plant growth samples being misclassified as background. The feature similarity between plant growth and background leads to a high confusion rate, indicating that the model's ability to distinguish between background and other types of damage needs to be improved.

Overall, the 300th epoch model slightly regressed in the detection of the plant growth category but performed stably in terms of the gray brick efflorescence category. The confusion problem between the background and other types of damage still exists, indicating that although increasing the number of training rounds can improve the performance of the model to a certain extent, overtraining may lead to the overfitting of certain features, thereby affecting the recognition effect of other categories. In the future, it may be necessary to find a more appropriate balance between the number of training rounds and the generalization ability to optimize the overall performance of the model in each category.

In summary, through the testing of the 23rd epoch, 170th epoch, 204th epoch, and 300th epoch models and detailed analysis of the confusion matrix, this study found that the 170th epoch model performed best in the overall performance, with balanced average precision, recall, and F1 score, especially in the recognition of two types of damage: alkali and plant growth. This shows that in the training process of the YOLO model, the appropriate number of training rounds and the reasonable adjustment of the hyperparameters can significantly improve the detection performance of the model.

In contrast, the 23rd epoch model performed poorly in the initial training, with serious false detection and missed detection, which is related to the fact that the model has not fully learned the target features. Although the 204th epoch and the 300th epoch models improved the recognition of specific categories in the later stages of training, they also showed a certain overfitting phenomenon, which aggravated the confusion problem of the background and other categories.

In the entire training and optimization process of the YOLOv8 model, the quality of the data annotation and the diversity of the samples have been shown to have a crucial impact on the detection performance of the model. Through multiple experiments and adjustments, the researchers found that model-assisted annotation (MAL) and moderate hyperparameter tuning are effective ways to improve the model performance. In addition, reducing complex data augmentation methods and maintaining a moderate amount of high-quality training samples are the key to improving the model detection accuracy under limited resources.

5.4. Comparison of Detection Results

Figure 23 illustrates how the four models—the 23rd epoch, 170th epoch, 204th epoch, and 300th epoch—display distinct characteristics in their efflorescence and plant growth detection results on the gray brick surface. This section analyzes the detection performance of the different models in detail, including instances of false and missed detection and the possible reasons for this.

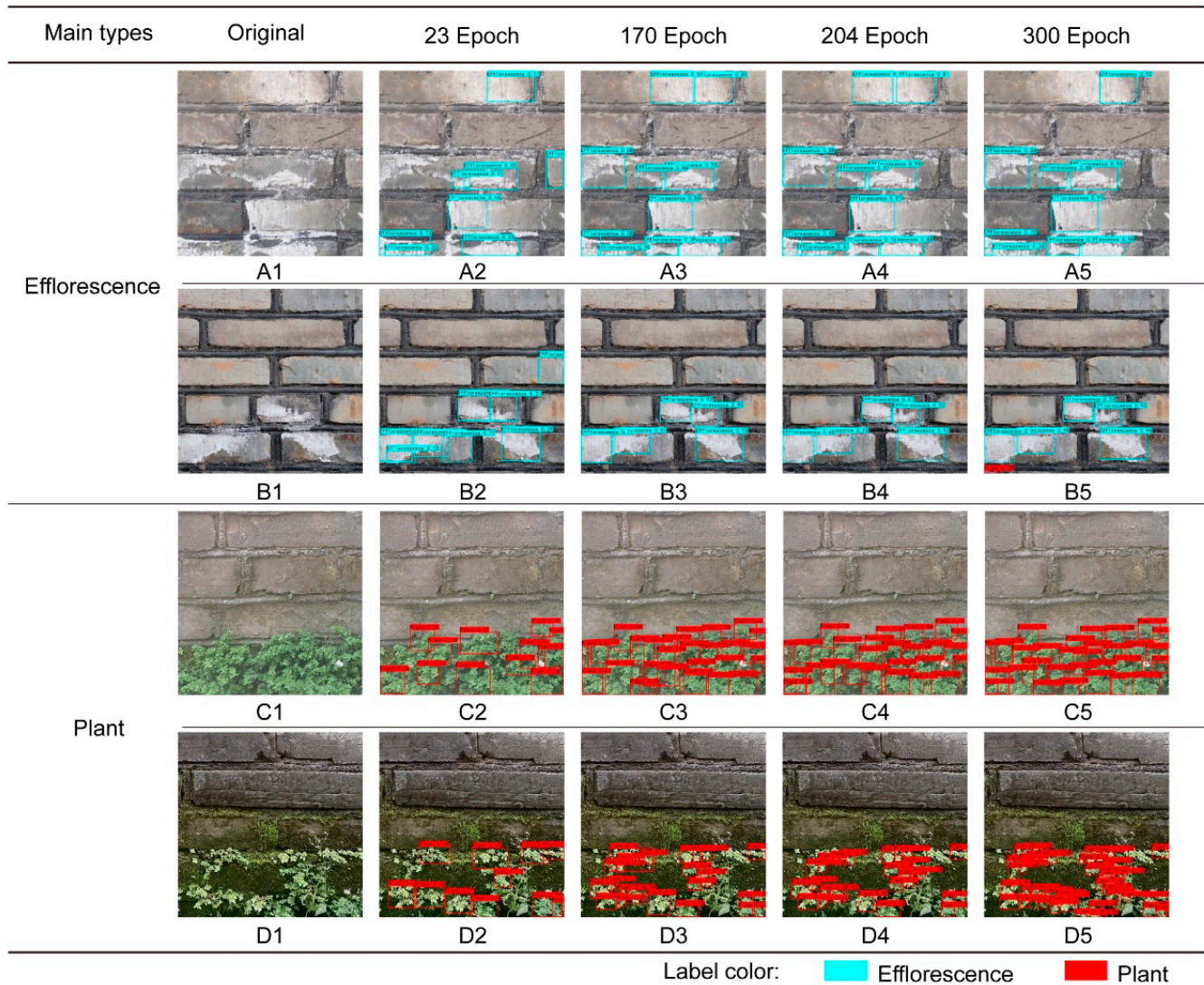


Figure 23. Analysis of the detection results of the different epoch models (image source: drawn by the author).

In the detection of efflorescence, each row shows the original image and the detection results of the four models at different generations. Fluorescent blue marks the detection label, indicating the efflorescence area of the gray brick. The detection results of the different models are analyzed as follows.

(1) Model of the 23rd epoch (A2, B2): The 23rd epoch model clearly exhibits a phenomenon of missed efflorescence area detection. Specifically, in Figure 23, A2 fails to identify some efflorescence areas, particularly those in the slightly lighter part of the gray brick's surface. This may be due to the small number of training generations, which leads to the model's failure to fully learn the various characteristics of efflorescence, especially its performance under different lighting and material conditions.

(2) Model of the 170th epoch (A3, B3): The 170th epoch model significantly enhances the efflorescence detection, detecting the majority of efflorescence areas and significantly reducing the phenomenon of missed detection. The figure demonstrates that the model accurately marks the larger efflorescence area, and its detection of the edge part is relatively accurate, suggesting that it has successfully learned the efflorescence features. The model can adapt well to the morphology and distribution of different efflorescences, which is the result of the parameter adjustment and enhanced feature extraction ability during training.

(3) Model of the 204th epoch (A4, B4): The performance of the 204th epoch model in TERMS OF efflorescence detection is comparable to that of the 170th epoch model, and it can cover the efflorescence area well.

(4) Model of the 300th epoch (A5, B5): The 300th epoch model is slightly inferior to the 170th epoch model in efflorescence detection. While the overall detection effect remains strong, the model misidentifies some efflorescence areas in B5 as areas of plant growth. This shows that in the later stage of training, the overfitting of some detailed features of the model may affect its generalization ability; especially in complex backgrounds, the detection accuracy of the model is slightly reduced.

In the detection of plants, the red mark indicates the detection result concerning plant growth, which shows the recognition effect of the model on the plant coverage area on the gray brick. The detection results of different models are analyzed as follows.

(1) Model of the 23rd epoch (C2, D2): The 23rd epoch model exhibits a significant number of missed detections and false detections when it comes to plant growth detection. Particularly in C2 and D2, the model incorrectly marks many obvious plant areas and mistakenly identifies some non-plant areas as plants. This may be due to the insufficient learning of plant features in the initial training stage of the model and the complex morphology of plant growth, which make the model incapable of distinguishing plants from gray brick backgrounds.

(2) Model of the 170th epoch (C3, D3): The 170th epoch model performs best in the detection of plant growth. The model correctly identifies most plant areas and significantly reduces the false detections. For example, in C3 and D3, the model can mark all the plant areas more accurately and has fewer false positives for the background. This shows that the 170th epoch model has made great progress in plant feature extraction and has good recognition abilities for complex plant morphology.

(3) Model of the 204th epoch (C4, D4): The 204th epoch model is close to the 170th epoch model in plant detection but performs slightly worse in the detection of some edge areas. In D4, the model fails to fully detect some plant areas, particularly small plant leaf edges. This may be because the model pays more attention to large-scale features than small-scale details during training in the 204th epoch, resulting in the missed detection of edge parts.

(4) Model of the 300th epoch (C5, D5): The plant detection effect of the 300th epoch model is improved compared with the 170th epoch and 204th epoch models. The C5 and D5 models reduce the omission of plant areas and successfully select more plants. The overfitting of features in the later stage of model training may be the cause of this situation, leading to obvious deviations in the model's ability to detect efflorescence and plant growth. The ability to detect efflorescence is weakened, while the ability to detect plant growth is enhanced, resulting in an obvious imbalance in the model.

By comparing the detection results of the four models, we can draw the following conclusions.

(1) Efflorescence detection: The 170th epoch and 204th epoch models performed best in terms of efflorescence detection and were able to effectively identify most efflorescence areas, with fewer false detections and missed detections. However, the 23rd epoch efflorescence model had a serious missed detection problem due to its insufficient feature extraction capability in the early stage of training. The 300th epoch model was not as stable as the 170th epoch model in processing edge details and had obvious false detections.

(2) Plant growth detection: The 170th epoch model performed well in plant growth detection, effectively distinguishing plants from backgrounds with fewer false and missed

detections. In contrast, the 23rd epoch model had the worst detection effect, with a large number of missed detections and false detections. The 204th epoch model was not effective at detecting edge areas, especially when the background was complex. The 300th epoch model performed best in the detection of plant growth, but considering the obvious false detection in the efflorescence test, the model's stability was poor.

(3) Overall performance: The 170th epoch model performed well in the detection of both types of damage, with high detection accuracy and stability. This shows that appropriate training generations and parameter adjustments can significantly improve the detection performance of the model. Future research could consider further optimizing the model's feature extraction capabilities, particularly in reducing false detections and improving the edge detection accuracy, to enhance the automated detection of gray brick damage in Fuzhou's ancient houses.

6. Discussion

6.1. Analysis of Model Feature Layers

An important way to determine how well the YOLOv8 model works at finding gray brick efflorescence is to look at the model feature layer visually. The efflorescence problem of gray brick surfaces in ancient houses in Fuzhou was the focus of this study, which analyzed the model's different feature layers to explore, in some depth, how the model extracts and focuses on the features of gray brick efflorescence during the detection process. By performing this analysis, we can obtain a better idea of what role each convolutional layer plays in feature extraction, especially when it comes to how accurate the detections are and how hard they are to recognize. This analysis also gives us a theoretical foundation for using the model in the future.

As shown in Figure 24, the feature map of the cv2 layer of the model in the gray brick efflorescence detection process shows the performance of the model in the primary feature extraction process. It is evident from cv2[0], cv2[1], and cv2[2] that the model reacts robustly to the edge features of the gray brick efflorescence area. The cv2 layer mainly captures the changes in the texture and edges of the gray brick surface. These low-level features are of enormous significance for the preliminary identification of the efflorescence area. The feature map reveals that the model extracts the high-brightness and edge parts of the image more accurately, particularly in areas with strong contrast. The response of the model is very obvious, which shows that the cv2 layer performs well in extracting the overall outline of the efflorescence feature. In addition, the cv2 layer also strongly annotates the parts with obvious brightness differences on the gray brick surface. These features help the model to further focus and refine the extraction of the efflorescence area in the subsequent convolutional layers.

In contrast, the cv3 layer is responsible for extracting higher-order features, including the complexity of local textures and some small-scale detail features. From cv3[0], cv3[1], and cv3[2], we can see that the cv3 layer has a more refined response to the smaller parts of the efflorescence area, especially on the bright spots inside the efflorescence area, where the model's reaction is very obvious. These high-level features extracted by the cv3 layer enable the model to further identify the detailed changes in the efflorescence area and effectively distinguish the differences between different efflorescence areas. For example, in the cv3[0] and cv3[1] feature maps, the model's response to small patches of efflorescence is prominent, especially for those irregular and scattered efflorescence areas. The model's detection performance in this layer is significantly better than that in the cv2 layer. These feature extractions not only make the model more adaptable to the detection process of efflorescence but also improve the ability to accurately locate it.

In the model, the feature fusion stage integrates the feature maps of different convolutional layers (cv2 and cv3 layers) to achieve comprehensive utilization of multi-scale information. This fusion strategy enables the model to capture low-level edge and texture features, as well as high-level semantic information, thereby improving the accuracy and robustness of the target detection. Specifically, YOLOv8 adopts the architecture of the feature pyramid network

(FPN) and the path aggregation network (PANet) to fuse feature maps of different scales. The FPN transfers high-level semantic features to low-level feature maps through a top-down path; the PANet enhances the contribution of low-level features to high-level features through a bottom-up approach. This bidirectional fusion mechanism enables the model to better balance global information and local details when detecting targets of different sizes and shapes. In the feature fusion process, the feature map of the cv2 layer mainly contains low-level edge and texture information, while the feature map of the cv3 layer contains higher-level semantic information. By fusing the features of the cv2 and cv3 layers, the model can simultaneously use edge, texture, and semantic information to provide a more comprehensive description of the target area. At the feature fusion stage, the fused feature map shows the effective integration of cv2 and cv3 layer features. By fusing features extracted from different levels, the model can use both low-level and high-level features, thereby accounting for both overall contours and detailed features during the detection process. This feature fusion mechanism is one of the keys to the YOLOv8 model’s ability to achieve high-precision target detection. The feature fusion map reveals a significant enhancement of the efflorescence area’s highlights, demonstrating the model’s increased attention to these areas. This shows that through feature fusion, the model can locate the efflorescence area more accurately, especially in the identification of the edges and center parts. Feature fusion can significantly improve the model’s detection ability.

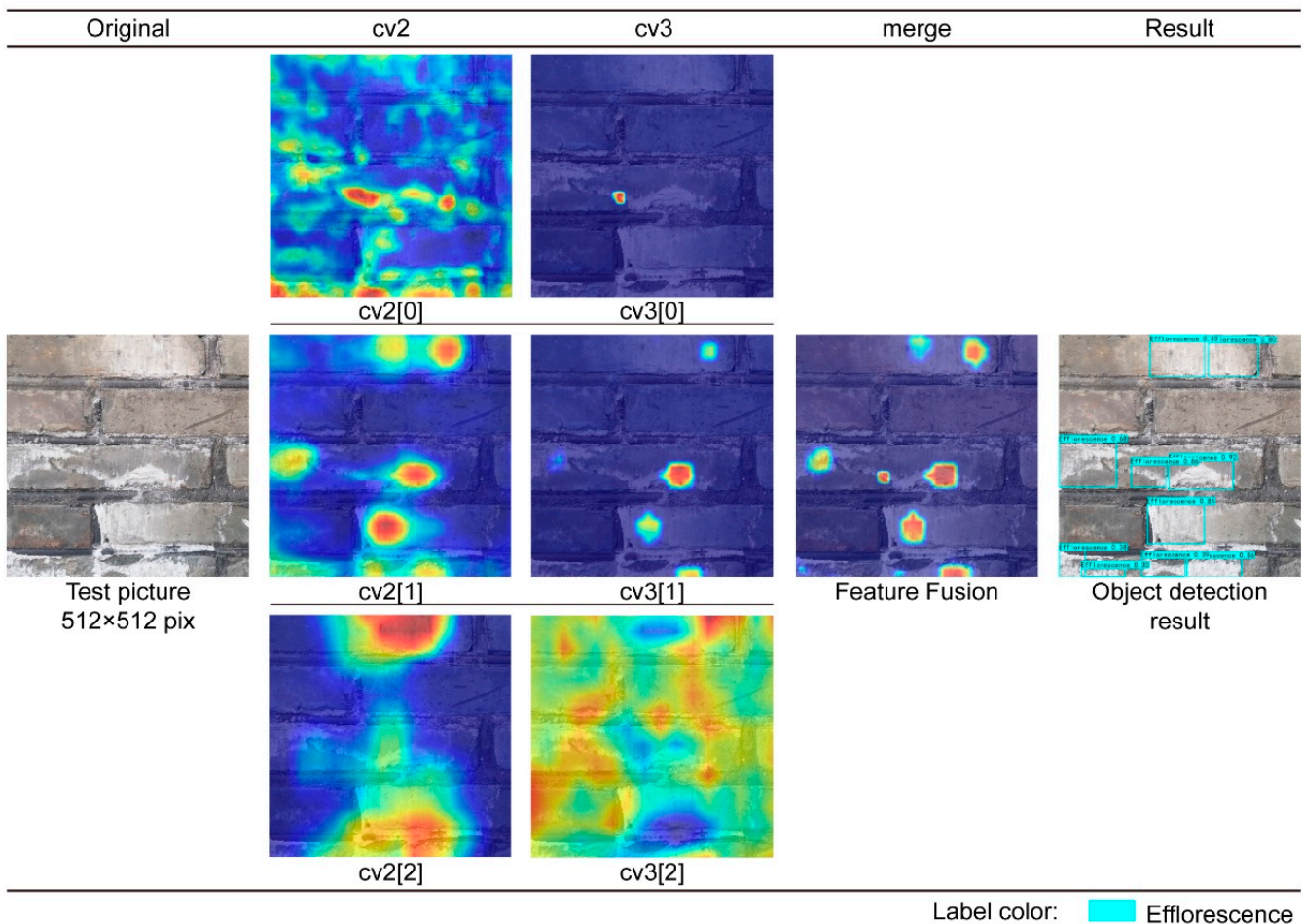


Figure 24. Feature map analysis of the model in the process of gray brick efflorescence detection (image source: drawn by the author).

Lastly, the final detection results demonstrate the overall effectiveness of the YOLOv8 model in detecting efflorescence on the gray brick surface. In the annotation results, the area marked with fluorescent blue is the efflorescence area identified by the model.

The model demonstrates a relatively accurate ability to detect most efflorescence areas, with a fairly complete recognition of the edge parts. The model makes good use of the results of the previous feature extraction and feature fusion in the detection process. It can tell the difference between the area with efflorescence and the background that is more complicated. This result proves that the previous feature layer extraction worked, showing that the YOLOv8 model can fully understand the different forms of gray brick efflorescence by extracting features and combining different convolutional layers, which leads to more precise and accurate detection in real life.

As shown in Figure 25, compared with the feature map analysis of gray brick plant growth and gray brick efflorescence detection, the detection of plant growth shows some obvious differences in feature extraction. These differences come from the difference in visual expression between plant growth features and efflorescence features.

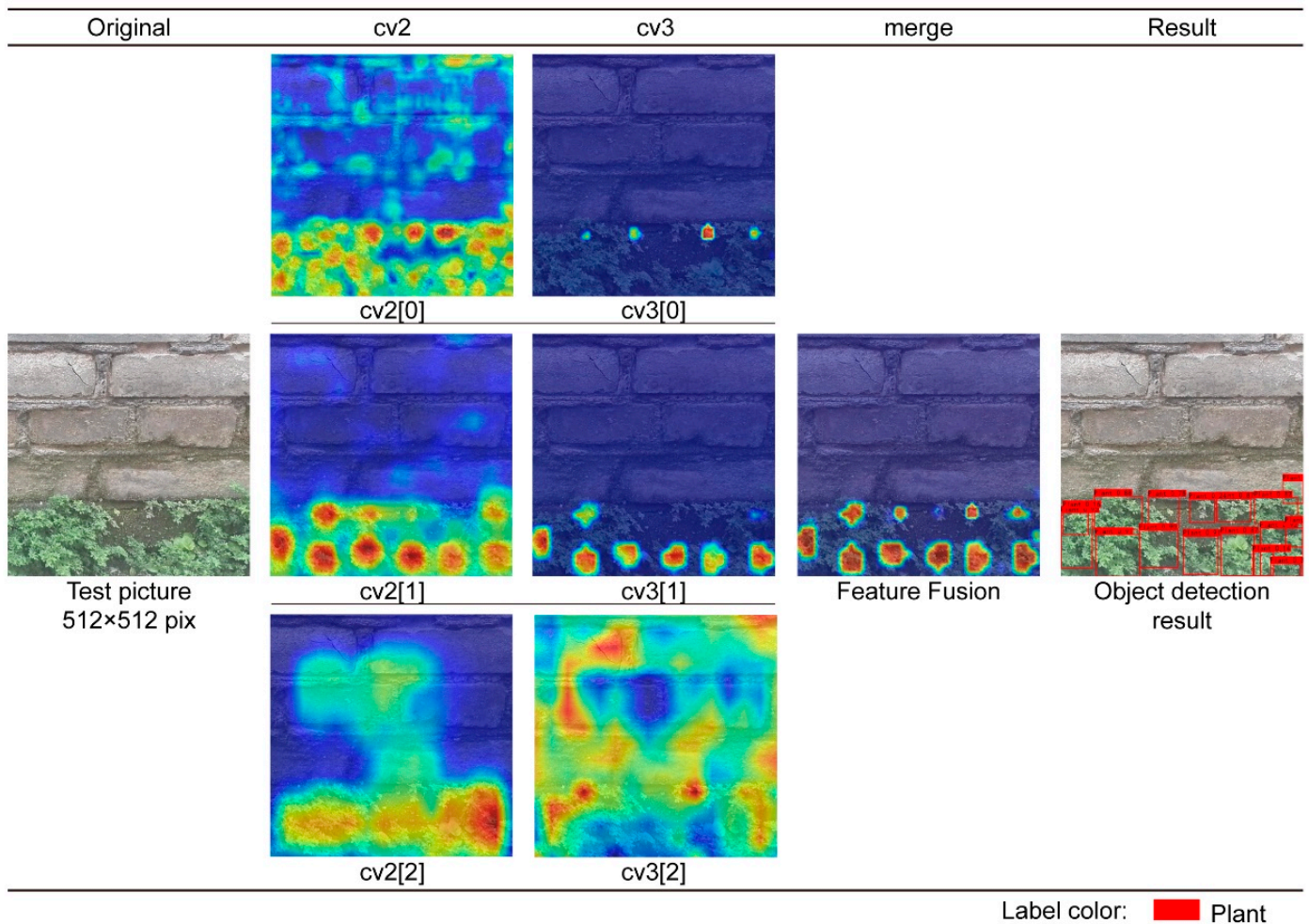


Figure 25. Feature map analysis of the model in the process of gray brick plant growth detection (image source: drawn by the author).

First, by observing the feature maps of the cv2 layer (cv2[0], cv2[1], cv2[2]), we find that the model’s feature extraction of plant growth areas shows different characteristics from its efflorescence detection. The cv2 layer concentrates the model’s response to the plant area in the lower half of the image, particularly in the denser plant growth area, where a large number of bright spots appear in the feature map. This demonstrates that the cv2 layer primarily concentrates the extraction of low-level features, such as texture and brightness changes, in the higher-contrast parts at the edge of the plant growth area. Compared with the efflorescence feature, the edge features of plant growth are more obvious, and the

texture complexity of the leaves is higher, so the model shows a strong response to these parts in the cv2 layer.

In the feature maps of the cv3 layer (cv3[0], cv3[1], cv3[2]), the model pays more attention to the overall distribution pattern and local complexity of plants, especially with a higher response to dense areas of plant communities. The model accurately captures small plant areas and leaf morphology in cv3[0] and cv3[1], reflecting the diversity of plant growth characteristics. The cv3 layer is more suitable for processing the local complexity of plant characteristics. The model can distinguish the boundaries of different plant parts at this layer and reduce misjudgment. In cv3[2], the model's response coverage of the entire plant area is relatively uniform, which allows the model to better distinguish plants from the gray brick background.

Therefore, the feature fusion graph shows the effective combination of different feature layers, especially in the identification of plant community boundaries. By fusing the features of the cv2 and cv3 layers, the model can more comprehensively identify the range of plant growth. In plant detection, feature fusion is particularly important for the extraction of edge details because plants usually have complex edge structures, and the fused features can more accurately mark these areas. In the final detection results, the model marks the plant growth area in red. The model accurately detects most of the plant area and reasonably marks the plant growth at the edge. The model's ability to effectively capture plant leaves, boundaries, and overall morphology during feature extraction significantly contributes to this. Unlike efflorescence features, plant growth has a more obvious spatial distribution and edge contours, and the model's effective extraction of these features ensures the accuracy of the detection results.

6.2. Model Application

6.2.1. Detection Process for Efflorescence of Gray Brick Surface

At the model application stage, this study conducted a detection experiment on high-resolution original images (4000×3000 pixels) taken with mobile phones to further verify the performance of the YOLOv8 model in actual scenes. By analyzing the detection feature map of efflorescence on the gray brick surface, we can observe changes and differences in the model's ability to extract efflorescence features under various resolutions and lighting conditions, as illustrated in Figure 26.

Judging from the feature maps of the cv2 layer (cv2[0], cv2[1], cv2[2]), the model's response to the efflorescence area of gray brick is different from that in previous experiments. In the detection of high-resolution original images, the feature maps of the cv2 layer show more refined edge features, which indicates that the model captures low-level features in large-scale images, such as texture and brightness changes, in more detail. Compared with previous experiments, the cv2 layer shows more obvious local area responses in this scene, especially in the efflorescence area at the bottom of the image, where the model's response is denser and brighter. This phenomenon may be due to the richer details in high-resolution images, which enable the model to extract efflorescence edge features at a finer scale.

In the feature maps of the cv3 layer (cv3[0], cv3[1], cv3[2]), the model's extraction of high-level features focuses more on the overall distribution and morphology of the efflorescence region. In particular, in cv3[0], the model shows a strong response to multiple small areas of efflorescence and can better distinguish efflorescence from undamaged gray brick. In cv3[1], the model captures the brightness changes in the efflorescence region and shows a response to the internal structure of the efflorescence region. The model is better at separating different efflorescence features when the resolution is high compared to the last experiment. It is especially good at noticing small changes in the edge and center of the efflorescence.

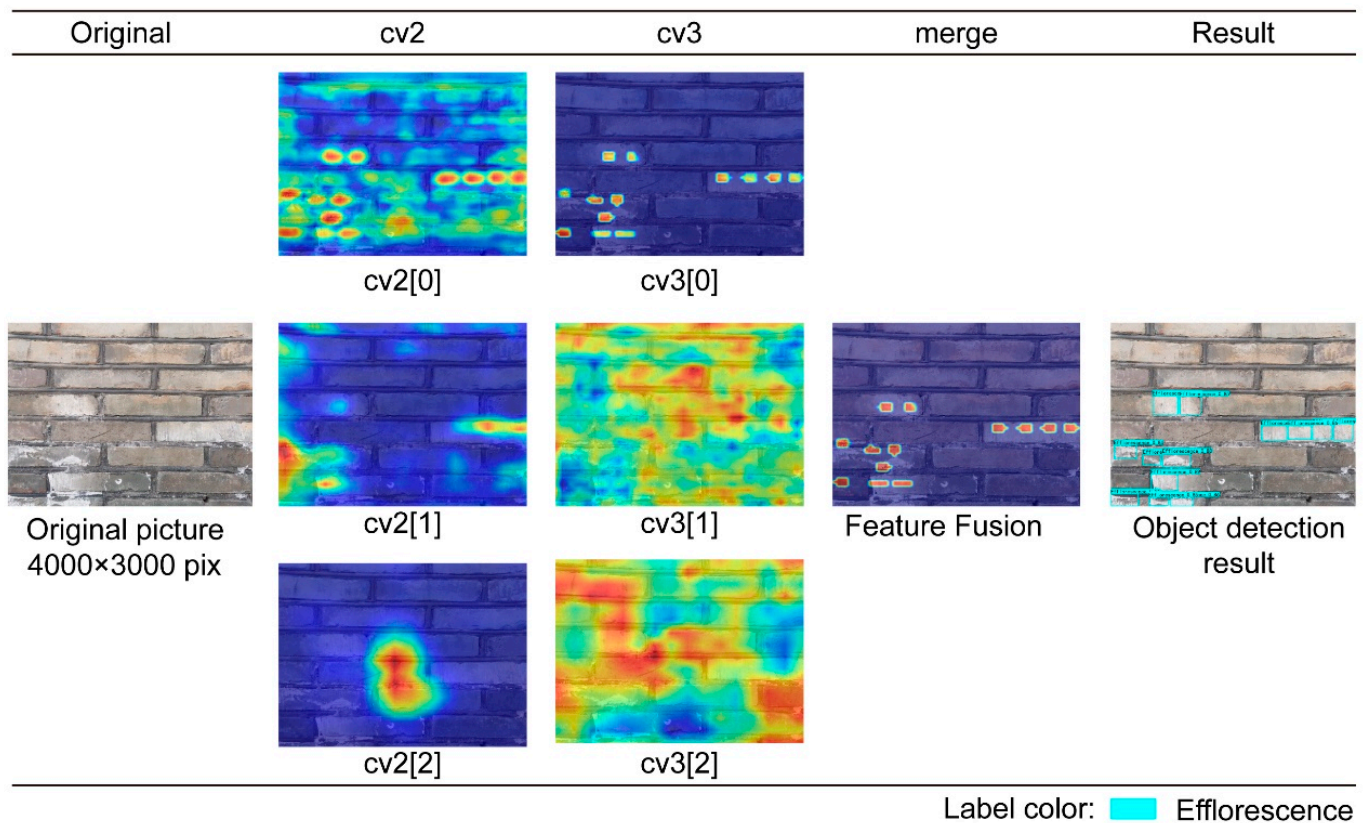


Figure 26. Feature map of the model's original image detection process for gray brick efflorescence (image source: drawn by the author).

At the feature fusion stage, the fused feature map shows the model's effective integration of features at different scales in high-resolution scenarios. The model can find more efflorescence areas and identify their boundaries more accurately by combining the fine-tuned extraction of low-level features with the overall distribution of high-level features. This feature fusion is particularly important under high-resolution conditions because the model needs to take into account both detailed features and overall features to ensure the accuracy of the detection results.

The final object detection result shows the performance of the YOLOv8 model in actual application scenarios. The results demonstrate the model's ability to accurately mark the efflorescence area on the gray brick surface, particularly in detecting complex efflorescence morphology. This verifies the generalization ability of the model in high-resolution images. Even when facing the original image with a complex background and different lighting conditions, the model still has strong detection accuracy and reliability.

6.2.2. Detection Process for Plant Growth on Gray Brick Surface

In terms of the detection of gray brick plant growth, it can be seen from the feature map in Figure 27 that the response of the cv2 layer to the plant growth area is mainly concentrated in the part below the image close to the ground. This is because the plant grows in a low position and has a significant texture difference with the background. In the high-resolution scene, the feature map of the cv2 layer (cv2[0], cv2[1], cv2[2]) displays more detailed edge and texture features, particularly for the plant's leaves and stems, where the model's response is more prominent. Because the high-resolution image contains more detailed information, the cv2 layer can capture the shape of the plant's leaves and the boundary between it and the gray brick background, thereby enhancing the recognition of the feature.

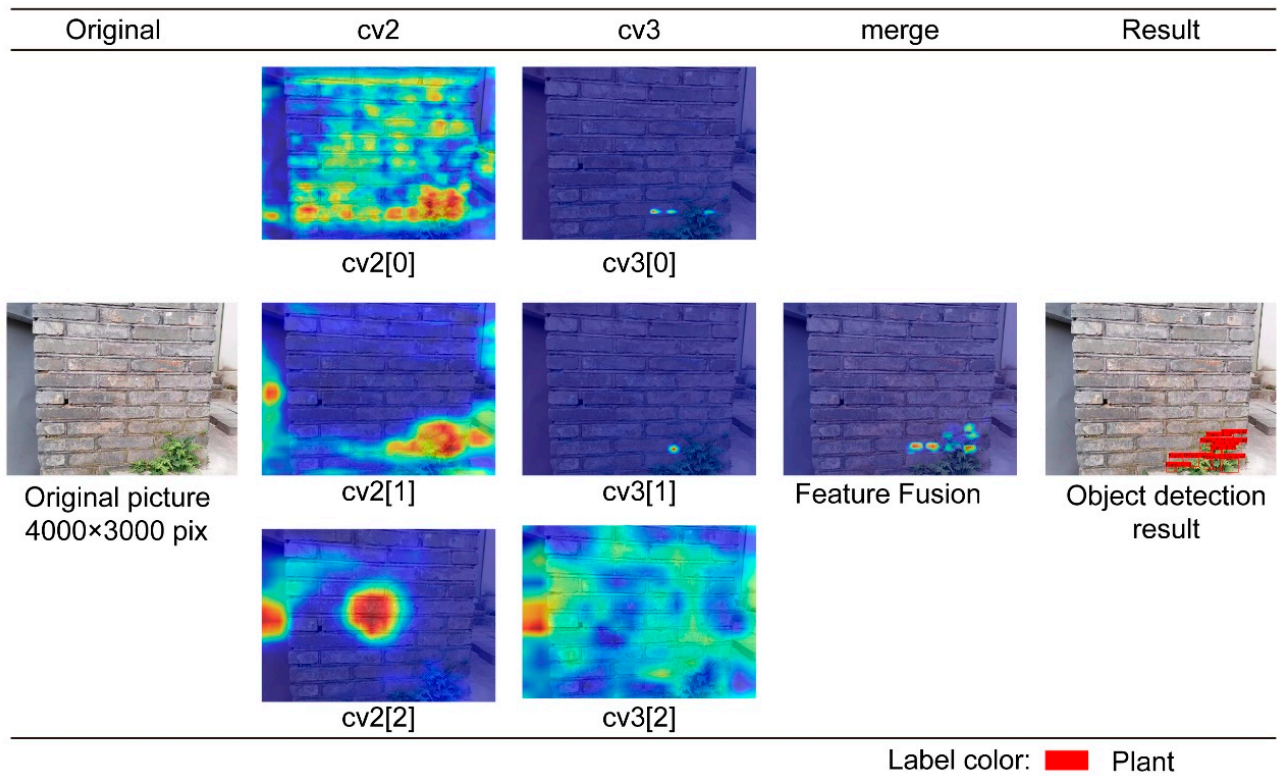


Figure 27. Feature map of the model’s original image detection process for gray brick plant growth (image source: drawn by the author).

The feature maps of the cv3 layer (cv3[0], cv3[1], cv3[2]) focus on the overall distribution of the plant growth area and the local morphological characteristics. The cv3[0] feature map displays the highlighted response to specific areas of the plant, particularly the more prominent parts. The model can identify the fine features of the plant in this layer. The feature maps of cv3[1] and cv3[2] show the brightness changes in the plant growth area and the contrast with the gray brick wall. Compared to efflorescence detection, the characteristics of plant growth are more complex, with significant uncertainty in the shape and density of the plant in the image. Therefore, the extraction of these complex features by the cv3 layer is particularly important. Especially under high-resolution conditions, the model shows a high sensitivity to the overall morphology of the plant, which helps to reduce missed detections during the detection process.

The feature fusion graph shows the comprehensive performance of different scale features extracted by the cv2 and cv3 layers. By fusing low-level features with high-level features, the model can more accurately locate and identify plant growth areas. The feature fusion graph demonstrates a further enhancement of the plant growth area, particularly in the dense leaf area. The fused features effectively combine edge and detail information, providing a more reliable basis for the final detection.

In the final detection results, the model marked the area of plant growth on the gray brick surface in red. From the detection results, we can see that the model recognizes the plant area accurately, especially in complex backgrounds, and can separate the plants from the background. The response of the cv3 layer confirms that, unlike the efflorescence feature, the detection of plant growth necessitates a robust local feature extraction capability in the model. The model’s detection results for plants prove its adaptability and effectiveness under high-resolution conditions and its ability to cope with the complex features of plants under different lighting and background conditions.

6.2.3. Extensive Field Testing

In the following experiments, we tested a large number of original gray brick images taken on site and used the YOLOv8 model to analyze the efflorescence and plant growth on the gray brick surface of the ancient houses in Fuzhou. Figure 28 shows the comparison between the original images and the test results in different scenes. Each group of photos indicates the model's detection of different types of damage. The following is a detailed description and analysis of each group of test results.

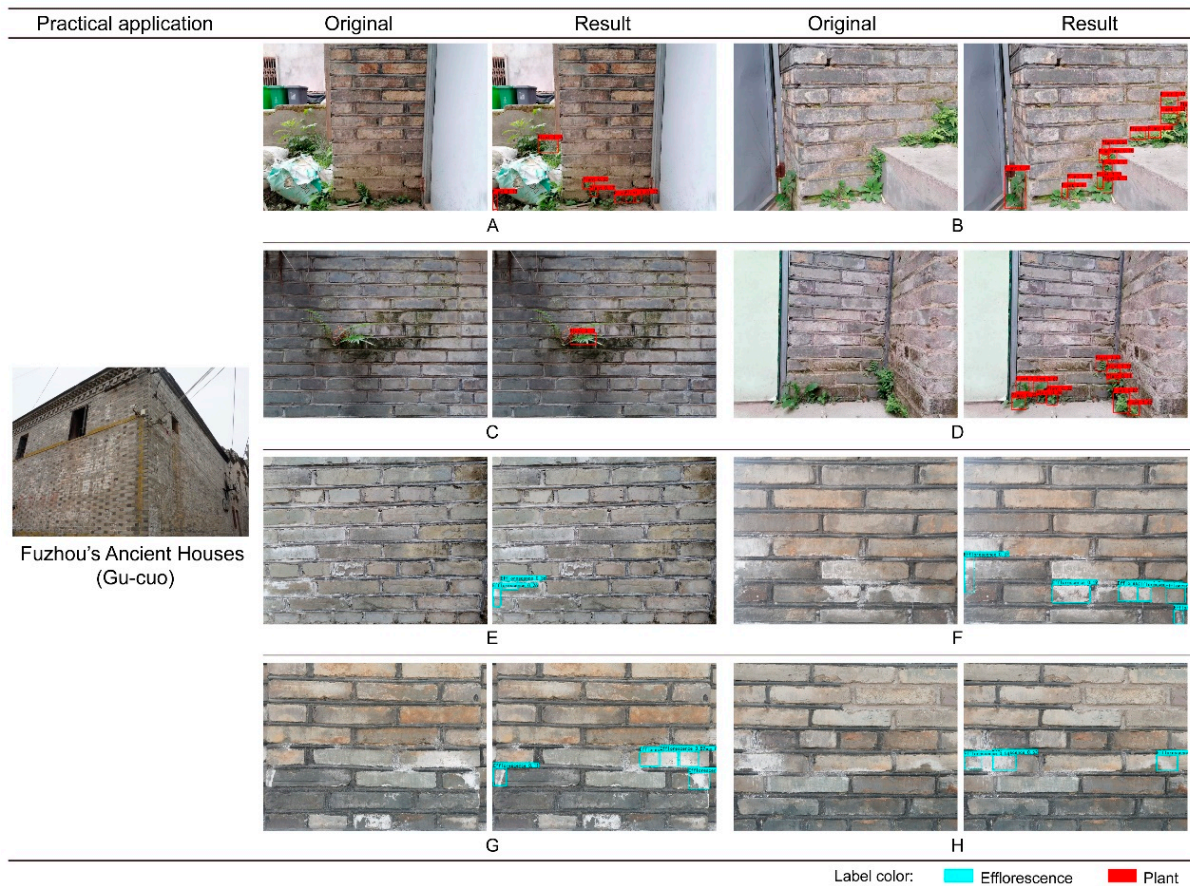


Figure 28. Testing of the model in field applications (image source: drawn by the author).

(1) A, B, C, and D in Figure 28 show that plant growth has been detected at the bottom of the gray brick wall. From the detection results, the YOLOv8 model accurately identifies the plant growth at the base of the wall, and the red mark shows the vegetation part that the model successfully detected. In particular, in Figure 28A, the model has a relatively complete annotation of multiple leaves and vegetation on the ground, showing excellent feature extraction capabilities. It is worth noting that in Figure 28B, the model has multi-level annotation of plant growth at the edge of the wall, which can capture the detailed features of the plants at the corners of the wall. This shows that in practical applications, the model has a strong ability to detect the edges and small parts of vegetation growth and can accurately distinguish plants from the wall background. In Figure 28D, the model successfully detects small plants growing in the brick joints, and the red annotation shows the effective recognition of these subtle growth areas. However, in Figure 28C, the model partially misses the plant growth area on the side of the wall. This could be attributed to the lighting conditions causing the plant color to blend in with the background wall color, thereby interfering with the model's recognition. This suggests that in practical applications, changes in illumination can significantly impact the model's detection performance, particularly when detecting small vegetation in complex backgrounds.

(2) E, F, G, and H in Figure 28 mainly show the model's detection of the efflorescence phenomenon on the gray brick surface. In the picture, the model marks the efflorescence area in cyan. E, F, G, and H in Figure 28 demonstrate the model's accurate identification of the efflorescence part of the gray brick surface, particularly its clear boundary marking. It is worth noting that the distribution of efflorescence on different bricks is not uniform, but the model can accurately detect the boundary and shape of these efflorescence areas, showing a satisfactory ability to extract efflorescence features. This shows that the YOLOv8 model has strong robustness in dealing with the efflorescence damage type and can still effectively identify it even when the efflorescence distribution is uneven. However, there are some missed efflorescence areas in the above pictures, especially those with lighter efflorescence colors and blurred boundaries. This shows that the model may have a certain degree of recognition difficulty when dealing with unclear efflorescence features. This experiment reveals that the saliency and contrast of features significantly influence the model's performance in efflorescence detection.

In general, the YOLOv8 model shows strong feature extraction and recognition capabilities when detecting plant growth and efflorescence on gray bricks in ancient houses in Fuzhou. When detecting plant growth, the model effectively captures plants at the bottom, edges, and gaps in the wall, particularly for vegetation parts with complex shapes and scattered distributions. When scenes have complex lighting or plant colors are close to the background, the model may miss some. In efflorescence detection, the model has a high detection accuracy for obvious efflorescence areas but may partially miss detections when efflorescence is unevenly distributed or the color is not obvious. The results of this study show that the YOLOv8 model has the potential to automatically detect damage to gray bricks in ancient buildings in Fuzhou in actual scenes, but it is also necessary to pay attention to the impact of factors such as ambient lighting and the significance of damage features on the detection accuracy.

6.3. Improvements Compared to Previous Studies

The method used in this study was compared with the detection method of Li, Q., et al. [66] and the traditional manual detection method in terms of the accuracy and time consumption in detecting efflorescence and plant growth categories. The specific data are shown in Table 2.

Table 2. Comparison of the present study methods with the results of other studies.

Method	Efflorescence Accuracy	Plant Accuracy	Time Required
Reference [66]	64.49%	97.00%	<0.05 min
This research	90.00%	45.00%	<0.05 min
Manual method	Depends on the person's professional level and experience		>1 min

Source: author's statistics.

As shown in Table 2, the proposed method has achieved a significant improvement in efflorescence efflux detection, reaching an accuracy of 90%, which is much higher than the 64.49% of the method of Li, Q., et al. [66]. However, in the detection of plant growth categories, the accuracy of this method is relatively low, only 45%, and there is still much room for improvement. In contrast, the method of Li, Q., et al. [66] performed better in plant detection, reaching an accuracy of 97%. Nevertheless, the detection time of both methods was kept within 0.05 min, which is significantly better than the traditional manual method.

The accuracy of the manual detection method depends on the professional level and experience of the detector, and it takes a long time, usually more than 1 min. This shows that the automatic detection method based on artificial intelligence has obvious advantages in terms of efficiency, especially for application scenarios that require rapid detection. In addition, the automatic detection method is stable and not easily affected by human factors, while the manual method may have fluctuations in the consistency of the results.

7. Conclusions

In this study, an automatic model to detect the main types of damage to the gray brick wall surface of ancient houses in Fuzhou, namely, gray brick efflorescence and plant growth, is constructed and applied. Using the YOLOv8 model, this study offers effective technical support and application examples for safeguarding Fuzhou's traditional architectural heritage. This is achieved through meticulous data processing, multiple experiments to optimize the model parameters, feature analysis in various environments, and application evaluation of the model in high-resolution real-life images. The results of this study not only verify the effectiveness of the YOLOv8 model in gray brick damage detection but also analyze the performance of the model under different training parameters and environmental conditions through a large number of experiments, leading to several key conclusions that help optimize the traditional building damage detection model.

(1) New understanding of coating science: The YOLOv8 model is used in this study to develop an automatic method to detect the surface damage of gray brick walls in ancient houses in Fuzhou, successfully identifying efflorescence and plant growth. Experiments show that the multi-scale feature fusion of YOLOv8 (such as the effective integration of cv2 and cv3 layer features) has significant advantages in terms of the detection accuracy, especially in areas with gray bricks with complex surface details. During the detection process, the model's accurate response to the edge of the efflorescence area and its effective recognition of irregular plant growth morphology verified the key role of feature fusion in the detection of building surface damage and provided a new technical reference for more accurate non-destructive detection methods.

(2) Application significance of this study: Through fine data processing and 10 experimental optimizations, strategies such as data enhancement, model-assisted annotation (MAL), and hyperparameter adjustment were explored, achieving an excellent performance with an mAP value of more than 0.5 in the final experiment. In the test phase, the model was trained on 512×512 pixel cropped images, and the detection effect was verified using high-resolution real-life images, showing a particularly strong robustness against complex backgrounds. In practical applications, the model provides efficient and accurate technical support for architectural heritage such as Fuzhou's ancient houses, with a detection speed of less than 0.05 min, effectively reducing the duration of manual detection.

(3) Scientific prospects: It was observed that the detection performance of the model fluctuates under different lighting conditions; in particular, when the light is weak or the plant color is similar to the background, false detection or missed detection is more likely to occur. To improve the adaptability of the model and to enhance its ability to cope with complex backgrounds, future research should further expand the scale of the dataset, including to different seasons and diverse environmental conditions. In addition, image preprocessing technology combined with illumination changes is expected to improve the generalization of the model, thereby promoting the application of computer vision technology in architectural heritage protection.

(4) Practical prospects: The detection model proposed in this study performs well for high-resolution images, but the efficiency of real-time detection in practice is still limited by computing resources. Future research can use model lightweighting techniques (such as pruning and quantization) to reduce the computational complexity of YOLOv8 and to improve its detection speed and real-time performance. In addition, the model can be extended to the detection of other types of building material damage to verify its effectiveness and versatility in a wider range of architectural heritage protection scenarios, providing broader application support for intelligent building detection technology.

Author Contributions: Conceptualization, L.Z. (Lei Zhang) and Y.C.; methodology, L.Z. (Liang Zheng); software, L.Z. (Liang Zheng); validation, L.Z. (Lei Zhang) and L.Z. (Liang Zheng); formal analysis, L.Z. (Lei Zhang) and Y.C.; investigation, L.Z. (Lei Zhang), B.Y., J.Z. and A.X.; resources, L.Z. (Lei Zhang); data curation, L.Z. (Lei Zhang); writing—original draft preparation, L.Z. (Lei Zhang), Y.C. and L.Z. (Liang Zheng); writing—review and editing, L.Z. (Liang Zheng); visualization, L.Z. (Liang Zheng), B.Y., J.Z. and A.X.; supervision, L.Z. (Lei Zhang) and Y.C.; project administration, L.Z. (Lei Zhang) and S.L.; funding acquisition, L.Z. (Lei Zhang) and S.L. All authors have read and agreed to the published version of the manuscript.

Funding: This research was funded by the Fujian Provincial Social Science Fund Project “Research on the Spatial Morphology of Ancient Capitals in the Minyue Region” (grant number: FJ2022C079); the Fujian Provincial Education and Research Project for Young and Middle-Aged Teachers (Science and Technology) “Research on Spatial Protection and Revitalization Strategies of Traditional Villages in Northern Fujian with Tourism as the Guide” (grant number: JAT190768); the Fujian Provincial First-Class Undergraduate Course “Architectural Surveying” (grant number: SJYLC202111); and the Ministry of Education Industry–University Cooperation and Collaborative Education Project “Construction and Practice of First-Class Courses in Information-Based Surveying of Architectural Heritage Based on PIE Software Support” (grant number: 220902313272006). Lei Zhang (zhanglei@wuyiu.edu.cn) is the leader of the above projects. Other people are also involved in the research. At the same time, this article was supported by the Key Laboratory of Smart Town Construction Technology in Hilly and Mountainous Areas of Fujian Universities. The funders had no role in the study conceptualization, data curation, formal analysis, methodology, software, decision to publish, or preparation of the manuscript. This study received no additional external funding.

Institutional Review Board Statement: Not applicable.

Informed Consent Statement: Not applicable.

Data Availability Statement: The datasets used and analyzed during the current study are available from Lei Zhang (zhanglei@wuyiu.edu.cn) on reasonable request.

Conflicts of Interest: The authors declare no conflicts of interest.

Appendix A. The Source of the Buildings in the Collected Photo Images

The tables below show the specific conditions of the buildings where the researchers collected photos. Also, due to the fact that these historical buildings have been renovated and have different styles, the number of samples collected from each building is inconsistent.

Table A1. No. 108 Wushan Road.


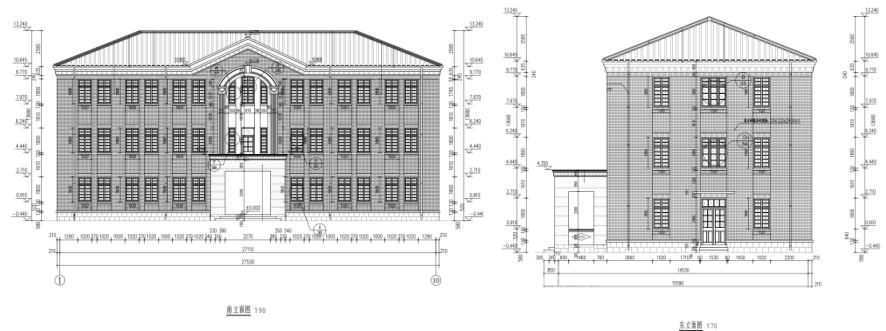
Value and Features	Meteorological Bureau Building No. 12 is located in the compound of the Southwest Provincial Meteorological Observatory on Wu Mountain. It covers an area of 425.60 m ² . Constructed in 1955, this three-story brick–concrete building faces southwards. The first floor features an entrance pavilion, while the middle of the second and third floors feature arched windows, simplified ancient Roman column decorations, and triangular pediments. The style of the two wings is simple, both with gray bricks. The offices on both sides, arranged in an inner corridor style with a cross-shaped traffic flow line, face the stairs at the entrance. The second floor features a skybridge that connects to Wu Mountain. The roof is a four-slope roof. This was an office building in the early days of the founding of the People’s Republic of China. It has a typical Soviet neoclassical style and has high historical and cultural value.
Building Name	Meteorological Bureau Building No. 12
Serial Number	350102_04_0002
Location of the Protected Area	Wushan Historic District
Address	No. 108 Wushan Road, Antai Street, Gulou District, Fuzhou City, Fujian Province
Era	After the founding of the People’s Republic of China
Announcement Batch	Fuzhou City’s fourth batch of historical buildings
Building Scope	

Table A1. Cont.

Surveying and Mapping



Source: The author’s statistics based on the field survey results.

Table A2. No. 151 Baima South Road.

Value and Features

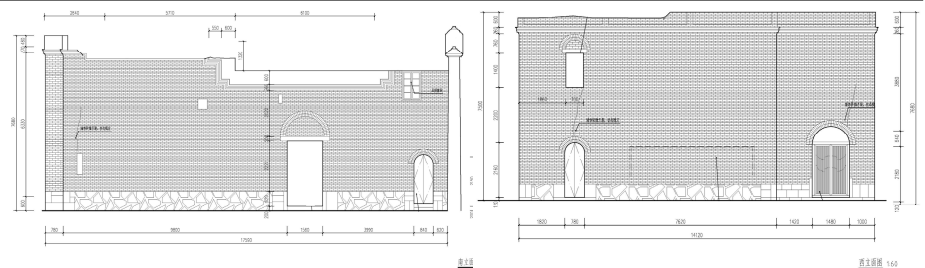
The former residence of the Wei family is a courtyard-style ancient dwelling, facing south and north, with a total area of about 204 m². The building has a courtyard facing the garden lane and shares walls with other courtyards on three sides. There is a single-arched door cover above the gate. Inside the gate, a corridor connects to the single-bay house on both sides, featuring a screen door in the middle. The main seat spans three bays and features a five-column flat corridor that extends to the front. The front eaves feature three arched jumps. Screen columns divide the main room into the front and rear halls. The master bedroom features a chessboard on its wall. There is a small patio behind the main seat. This building, a typical small dwelling in Fuzhou City, holds significant historical and cultural value.

Building Name	The former residence of the Wei family
Serial Number	350102_03_0005
Location of the Protected Area	Zhuzifang Historic District
Address	No. 60 Huayuan Lane, Taijiang District, Fuzhou City, Fujian Province
Era	Qing Dynasty
Announcement Batch	Fuzhou City’s third batch of historical buildings

Building Scope



Surveying and Mapping



Source: The author’s statistics based on the field survey results.

Table A3. No. 17 Tianhuangling Lane.

Value and Features	The building at No. 17 Tianhuangling Lane dates back to the early Qing Dynasty. It is an ancient courtyard-style residence, facing east and sitting west. The main gate is a tiger-head gate, with a height difference of 12 levels from the street. Entering the main gate leads to a pavilion on the left, which features a three-step water corridor and a spacious courtyard. The main seat is three bays wide and six columns deep, with a veranda. The main hall spans three bays and lacks a central column. The through-beam frame is designed in a simple style, with saddle walls on both sides of the hard mountain roof. The back courtyard is small, and the pavilion is only one bay. The building is relatively old and simple in style. The hall with beams and columns is of a higher level. It is more likely to be a family temple or ancestral hall with high historical and cultural value.
Building Name	No. 17 Tianhuangling Lane
Serial Number	350102_04_0001
Location of the Protected Area	Wushan Historic District
Address	No. 17 Tianhuangling Lane, Antai Street, Gulou District, Fuzhou City, Fujian Province
Era	Qing Dynasty
Announcement Batch	Fuzhou City's fourth batch of historical buildings

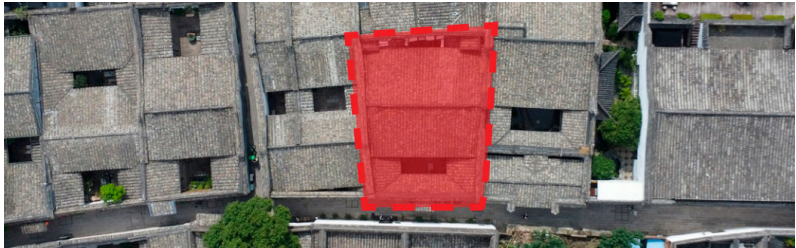
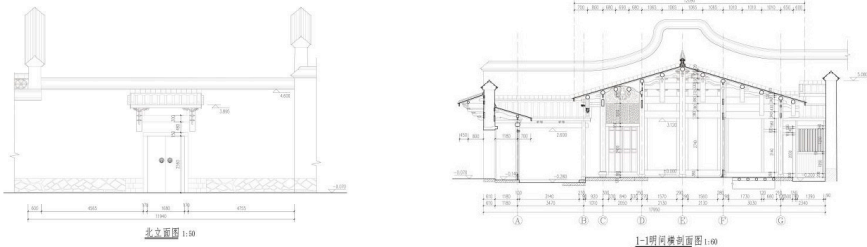
Building Scope

Source: The author's statistics based on the field survey results.

Table A4. No. 20 Daguangli.

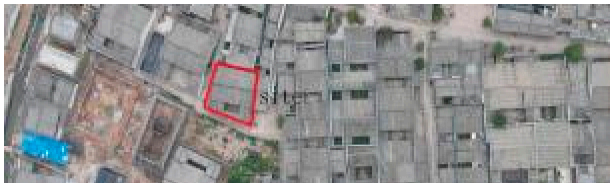
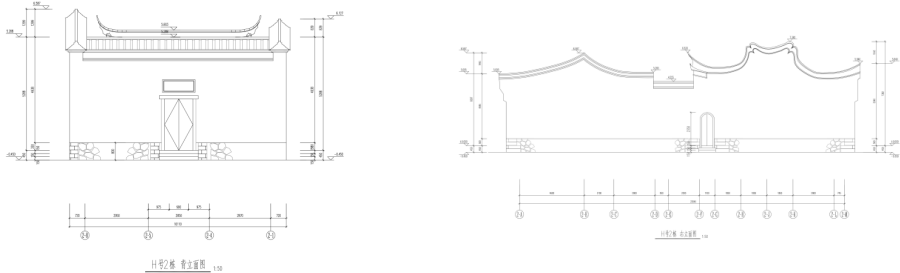
Value and Features	The building faces south and north, and the main entrance is located in Daguangli. The building faces Daguangli to the north and Huang Ren's former residence to the south. The building has two courtyards, consisting of a porch, two side corridors, a front patio, a main seat, a back patio, two side pavilions, and four walls. The north facade of the entrance is a door cover. The building connects the porch to the two side corridors and surrounds the front patio on three sides. Its main body is a through-beam frame, and the roof is a single-slope roof facing the patio. There is a screen door between the porch and the front patio. The main seat is single-story, with a width of three bays and a depth of five columns. The main beam frame is a through-beam frame, and the roof is a double-slope roof. An inserted arch cantilevers the cantilevered eaves, while the front eaves function as verandas. There are hanging flower columns under the eaves, and the rear eaves are hard cantilevered. The main seat veranda has exquisite carvings, such as the giant flowers and partition doors; the Dingtou arch under the purlin of the main room; the one-dou-three-sheng on the front column partition frame; and the Taishi wall on the rear column screen door. The pavilions on both sides of the back patio also feature through-beam main beams, and the roof is designed with a double-slope design. Stone strips pave the ground of the two patios. The plane layout, structural system, and detailed decoration prominently display regional characteristics, incorporating both contemporary and regional elements. The building follows a traditional courtyard-style design, and its exquisitely crafted roof tiles embody certain historical, artistic, and scientific values.
Building Name	No. 20 Daguangli
Serial Number	350102_05_0004
Location of the Protected Area	Three Lanes and Seven Alleys Historic District
Address	No. 20 Daguangli, Gulou District, Fuzhou City, Fujian Province

Table A4. Cont.

Era	Qing Dynasty
Announcement Batch	Fuzhou City's fifth batch of historical buildings
Building Scope	
Surveying and Mapping	


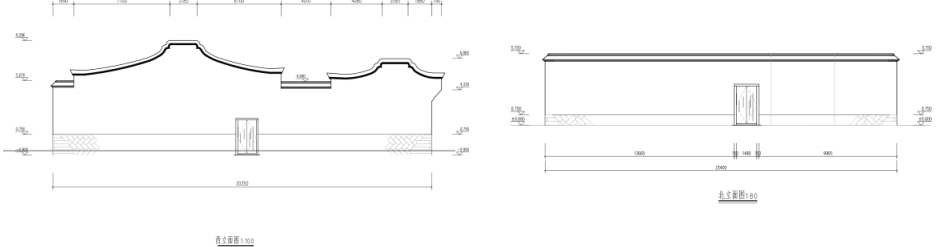
Source: The author's statistics based on the field survey results.

Table A5. No. 254 Dongguan Street.

Value and Features	The Qing Dynasty built the 391 m ² structure, which faces both east and west. It is a courtyard-style residence. The entrance hall, patio, pavilion, and main seat form the center of the plan. The main seat is five bays wide and five columns deep, with a through-beam structure and a granite mountain top. The square brackets, the exquisitely carved wall, and the simple and intact column base and other components are all representative features. The building is in excellent condition. Its axially symmetrical plan layout and exquisite decorative components highlight the characteristics of ancient Fuzhou residences in the Qing Dynasty and are of certain value to the study of local architecture and living culture.
Building Name	No. 254 Dongguan Street
Serial Number	350182-WH-025
Location of the Protected Area	Heping Street Historical Area
Address	No. 185 Heping Street, Wuhang Subdistrict, Changle District, Fuzhou City, Fujian Province
Era	Qing Dynasty
Announcement Batch	The second batch of historical buildings in Changle District, Fuzhou
Building Scope	
Surveying and Mapping	

Source: The author's statistics based on the field survey results.

Table A6. No. 172 Heping Street.

Value and Features	The building faces south and covers an area of 429 m ² . The Ming and Qing Dynasties built this courtyard-style residence. The plan revolves around the hall, encompassing the entrance hall, patio, pavilion, and main seat. The main seat is five bays wide and five columns deep, with a through-beam structure and a granite mountain top. The square brackets, the exquisitely carved wall, and the simple and intact column base and other components are all representative features. The building is in excellent condition. Its axially symmetrical plan layout and exquisite decorative components highlight the characteristics of ancient Fuzhou residences from the Ming and Qing Dynasties and are of certain value in studying local architecture and residential culture.
Building Name	No. 172 Heping Street
Serial Number	350182-WH-037
Location of the Protected Area	Heping Street Historical Area
Address	No. 172 Heping Street, Wuhang Subdistrict, Changle District, Fuzhou City, Fujian Province
Era	Qing Dynasty
Announcement Batch	The second batch of historical buildings in Changle District, Fuzhou
Building Scope	
Surveying and Mapping	

Source: The author's statistics based on the field survey results.

Table A7. No. 44 Jing Street.


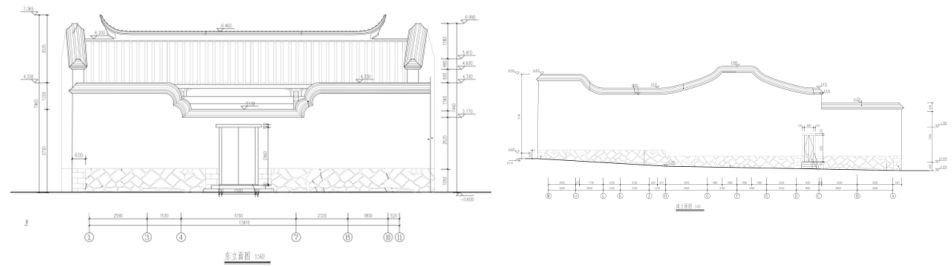
Value and Features	No. 44 Jing Street is located in Yijing Village, Wufeng Street, Gulou District, Fuzhou City, Fujian Province. The late Qing Dynasty built it. It is a courtyard-style ancient residence, facing west and east. The main body is a through-beam structure. The main seat is three bays wide and five pillars deep. The roof is composed of a hard mountain style. The overall appearance is average (partially renovated); the gables, brackets, column bases, etc., are well-preserved and exhibit a certain degree of representativeness.
Building Name	No. 44 Jing Street
Serial Number	350102_04_0007
Location of the Protected Area	Yijing Cultural Park
Address	No. 44 Jing Street, Yijing Village, Wufeng Street, Gulou District, Fuzhou City, Fujian Province
Era	Late Qing Dynasty
Announcement Batch	Fuzhou City's fourth batch of historical buildings
Building Scope	

Table A7. Cont.

Surveying and Mapping



Source: The author’s statistics based on the field survey results.

Table A8. No. 96 Fosi Lane.

Value and Features

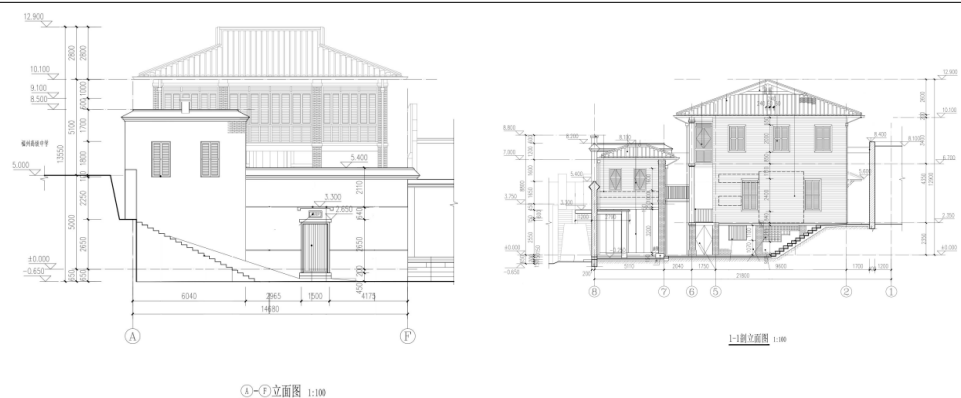
Kaiyinglu comprises a two-and-a-half-story main building and a two-story annex building, linked by stairs. This floor plan is very common in the Cangshan area, and it is estimated that the construction time was between 1900 and 1920. The internal layout of Kaiyinglu is quite special. The main building has an elevated ground floor, and the second floor is a Chinese-style hall with a screen door.

Building Name	Kaiyinglu
Serial Number	350102_03_0005
Location of the Protected Area	Yantaishan Historic District
Address	No. 96 Fosi Lane, Cangqian Street, Cangshan District, Fuzhou City, Fujian Province
Era	Between 1900 and 1920
Announcement Batch	Fuzhou City’s third batch of historical buildings

Building Scope

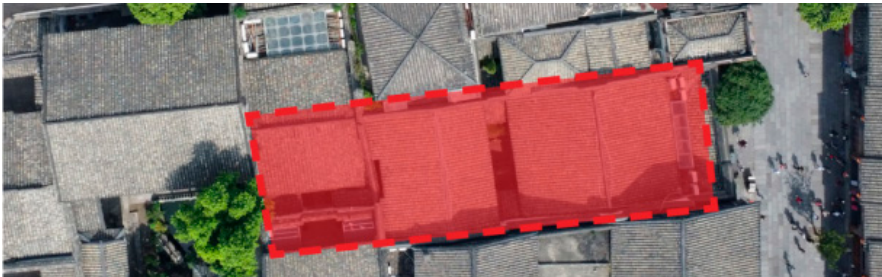
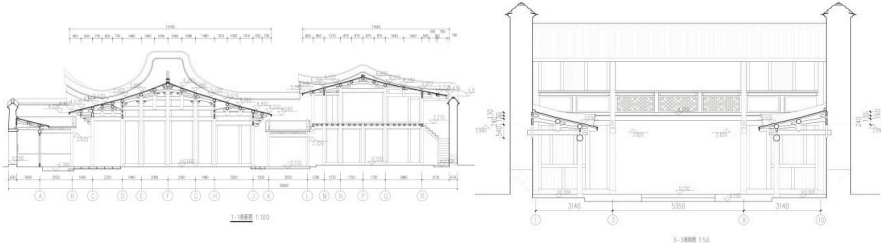


Surveying and Mapping




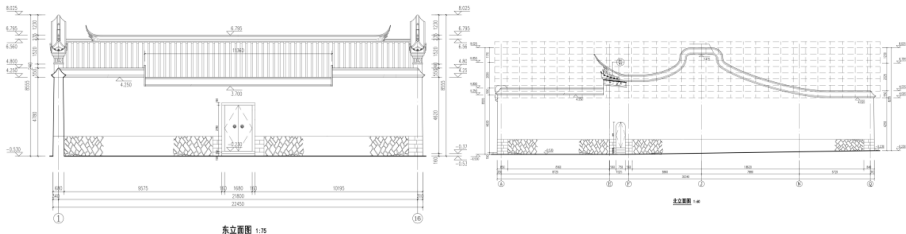
Source: The author’s statistics based on the field survey results.

Table A9. No. 50 Nanhou Street.

Value and Features	<p>The building has two courtyards, consisting of a porch, a patio, a main building, a patio, corridors on the north and south sides, a main building, and four walls. The main entrance is located on the east facade. The porch is single-story, surrounding the patio in a U shape. The main body is a through-beam frame, and the roof is a single-slope roof facing the patio. A steel-glass roof is added between the porch roof and the roof of the main building. The main building is single-story, with a width of three bays and a depth of seven columns. The main beam frame is a through-beam frame, and the roof is a double-slope roof. Both the front and rear eaves serve as verandas, featuring arches that protrude from them. The main building boasts exquisite carvings, including the Dingtou arch located beneath the purlin of the building, the one-beam, three-liter frame on the front column spacing frame, and the screen door. Stream buildings are situated on both sides of the main building. On the north and south sides of the patio, there are side corridors, and the corridors are adorned with beautiful backrests. The second entrance's main building spans two stories, boasting a width of three bays and a depth of five columns. The main beam frame is a through-beam frame, and the roof is a double-slope roof. The staircase is located at the back of the building. The second floor's front eaves serve as cantilevered corridors, while the west facade wall connects the back eaves. Square bricks pave the floors of the first and second main buildings, while stone strips pave the floors of the two courtyards.</p>
Building Name	No. 50 Nanhou Street
Serial Number	350102_05_0003
Location of the Protected Area	Three Lanes and Seven Alleys Historic District
Address	No. 50 Nanhou Street, Gulou District, Fuzhou City, Fujian Province
Era	Late Qing Dynasty
Announcement Batch	Fuzhou City's fifth batch of historical buildings
Building Scope	
Surveying and Mapping	

Source: The author's statistics based on the field survey results.

Table A10. No. 174 Nanhou Street.

Value and Features	The Qing Dynasty saw the construction of No. 174 Nanhou Street, which spans an area of approximately 577 m ² . It is a wooden structure, designed in the courtyard-style of an ancient residence. The main building is three rooms wide and seven columns deep. It faces south and sits north. The main body of the structure is made of through-beams, while the roof is a hard mountain roof. After repair, it is intact as a whole. The entrance to the main building is located in the southeast. There is a double-sloped screen door at the entrance. There is a pavilion in the front courtyard. The Taishi wall, carvings, and other components of the main building remain intact, making it a representative structure. The other building is situated in the northeast, facing both west and east. Only the main building is left. It is three rooms wide and four columns deep. The absence of a front eaves column is a unique feature of this building. This residence, located in the Three Lanes and Seven Alleys Historic District of Fuzhou, is one of the ancient Qing Dynasty residences, providing valuable physical materials for the study of Qing Dynasty residential architecture.
Building Name	No. 174 Nanhou Street
Serial Number	350102_03_0003
Location of the Protected Area	Three Lanes and Seven Alleys Historic District
Address	No. 174 Nanhou Street, Gulou District, Fuzhou City, Fujian Province
Era	Late Qing Dynasty
Announcement Batch	Fuzhou City's third batch of historical buildings
Building Scope	
Surveying and Mapping	

Source: The author's statistics based on the field survey results.

Appendix B. Machine Learning Runtime Environment

The operating system was Windows 11 (X64), the CUDA version was 11.5, the deep learning framework was PyTorch (1.13.0), and the graphics card and processor were a GeForce GTX 3070 (16 G) and an AMD Ryzen 9 5900HX (3.30 GHz), respectively.

References

1. The Cultural Context of Ancient Houses in FUZHOU. Available online: <http://fj.people.com.cn/BIG5/n2/2021/0722/c181466-34831662.html> (accessed on 31 August 2024).
2. Lan, X. Research on the Revitalization and Utilization of Traditional Ancient Houses in Fuzhou from the Perspective of Cooperative Governance. *J. Fujian Polytech. Norm. Univ.* **2024**, *42*, 59–64. (In Chinese) [CrossRef]
3. Lin, J. Research on the Protection and Restoration Technology of Cultural Relics Buildings: A Case Study of the West Flower Hall of Xiaohuanglou in the Three Lanes and Seven Alleys Historic District, Fuzhou. *Strait Sci.* **2024**, *6*, 92–95. Available online: <https://chn.oversea.cnki.net/KCMS/detail/detail.aspx?dbcode=CJFD&dbname=CJFDLAST2024&filename=YJYZ202406017&uniplatform=OVERSEA&v=4QE9itdmE250JPOv9ESOdDKtyPLtFLvI-4Sl8gzW3yZM4CeSpbMKn3SLH5MlmY-Y> (accessed on 10 November 2024). (In Chinese)

4. Liao, H.; Wu, S. Research on the Spatial Form and Decorative Patterns of Ancient Folk Houses in Eastern Fujian: Taking Nanyan Village in Fu'an City as an Example. In *Proceedings of the 4th International Conference on Architecture: Heritage, Traditions and Innovations (AHTI 2022)*, Online, 24–25 February 2022; Athena Publishing: Amsterdam, The Netherlands, 2023; pp. 153–161. [CrossRef]
5. Gu-Cuo in Fuzhou. Available online: <https://tv.cctv.com/2020/11/09/VIDAO48QSUUkZnMMpy2HeQx5201109.shtml> (accessed on 31 August 2024).
6. Ji, H. Research on the Protection and Revitalization of Ancient Houses in Fuzhou from the Perspective of Heritage: On the Value and Limitations of the “Technical Guidelines for the Protection, Renovation and Reconstruction of Historical Buildings in Fuzhou”. *New Archit.* **2024**, *1*, 81–85. Available online: <https://chn.oversea.cnki.net/KCMS/detail/detail.aspx?dbcode=CJFD&dbname=CJFDLAST2024&filename=XJZJ202401015&uniplatform=OVERSEA&v=r1MsuVeF3b5t52Ku-f34Qp5uG7yccmtaPRoNGVCUm3GgcX8GGkO-YqqKORSpAPL9> (accessed on 10 November 2024). (In Chinese).
7. Song, C. A brief analysis of the architectural structure of ancient residential buildings in Fuzhou. *Cult. Relics Apprais. Apprec.* **2023**, *12*, 89–93. (In Chinese) [CrossRef]
8. Wang, G. The Practice of Ancient House Protection and Urban Renewal in Fuzhou: A Case Study of the Three Lanes and Seven Alleys Historic District. *J. Fujian Educ. Inst.* **2023**, *24*, 32–35. Available online: https://chn.oversea.cnki.net/KCMS/detail/detail.aspx?dbcode=CJFD&dbname=CJFDLAST2023&filename=FJXB202304007&uniplatform=OVERSEA&v=-zQHivTF-j5ZhZLmNLavAc9NC7toWofChNrsDig4LKQG0nCqHC_WP-ISHsXpdc (accessed on 10 November 2024). (In Chinese).
9. Lan, W. Reflections on the Cultural Protection of Ancient Houses in Fuzhou: A Case Study of Sanfang Qixiang. *J. Party Sch. Fuzhou CPC Comm.* **2024**, *1*, 86–90. Available online: https://chn.oversea.cnki.net/KCMS/detail/detail.aspx?dbcode=CJFD&dbname=CJFDLAST2024&filename=FZDX202401012&uniplatform=OVERSEA&v=9Pp-dgw1Mo7QkhGeYn2MLT26RzXscFGsuiHPW8L_YJPw8JPe3EGv-zZx4VLCN7M (accessed on 10 November 2024). (In Chinese)
10. Du, J. Research on the Development Trend of Computer Science and Technology in the “Internet+” Era. *J. Phys. Conf. Ser.* **2020**, *1682*, 012070. [CrossRef]
11. Deng, J. Research on the integrated development of revitalization and study tour of ancient houses in Fuzhou. *J. Taiyuan Urban Vocat. Tech. Coll.* **2024**, *8*, 45–47. (In Chinese) [CrossRef]
12. Hang, S.; Ye, M.; Xu, Q.; Zhou, J.; Wu, J.; Yan, C. Study on the color gene characteristics of ancient houses in traditional villages in Fuzhou. *Urban Archit.* **2023**, *20*, 51–53. (In Chinese) [CrossRef]
13. Chen, S. Research on the Protection and Development of Ancient Houses in the Context of Rural Revitalization: A Case Study of Shuixilin Ancient Houses. *J. Cult. Stud.* **2023**, *2*, 40–43. Available online: https://chn.oversea.cnki.net/KCMS/detail/detail.aspx?dbcode=CJFD&dbname=CJFDLAST2023&filename=WHXU202302009&uniplatform=OVERSEA&v=se_rjN-834rGXDRAMSKUM7uSExtMqes5fzZuyMoGxt1rGr5TBltw9zrlGesCYK4M (accessed on 10 November 2024). (In Chinese)
14. Wang, X.; Gao, H.; Jia, Z.; Li, Z. BL-YOLOv8: An Improved Road Defect Detection Model Based on YOLOv8. *Sensors* **2023**, *23*, 8361. [CrossRef] [PubMed]
15. Bakirci, M. Enhancing vehicle detection in intelligent transportation systems via autonomous UAV platform and YOLOv8 integration. *Appl. Soft Comput.* **2024**, *164*, 112015. [CrossRef]
16. Farooq, J.; Muaz, M.; Khan Jadoon, K.; Aafaq, N.; Khan, M.K.A. An improved YOLOv8 for foreign object debris detection with optimized architecture for small objects. *Multimed. Tools Appl.* **2024**, *83*, 60921–60947. [CrossRef]
17. Casas, G.G.; Ismail, Z.H.; Limeira, M.M.C.; da Silva, A.A.L.; Leite, H.G. Automatic Detection and Counting of Stacked Eucalypt Timber Using the YOLOv8 Model. *Forests* **2023**, *14*, 2369. [CrossRef]
18. Gai, R.; Liu, Y.; Xu, G. TL-YOLOv8: A blueberry fruit detection algorithm based on improved YOLOv8 and transfer learning. *IEEE Access* **2024**, *12*, 86378–86390. [CrossRef]
19. Wang, Y.; Zhang, K.; Wang, L.; Wu, L. An improved YOLOv8 algorithm for rail surface defect detection. *IEEE Access* **2024**, *12*, 44984–44997. [CrossRef]
20. Liao, X.; Lin, W.; Cai, Y.; Wei, X. Analysis on the Development Strategies of Ancient House Cultural Tourism Industry in Fuzhou. *Strait Sci. Technol. Ind.* **2021**, *34*, 73–77. Available online: https://chn.oversea.cnki.net/KCMS/detail/detail.aspx?dbcode=CJFD&dbname=CJFDLAST2022&filename=HXKT20211017&uniplatform=OVERSEA&v=JYzpkOEhg0Jo_UxdjZIMnPvDxjsc_dmaR5AfkISzL5bV3flzsv4XGX6oorXFfjr (accessed on 10 November 2024). (In Chinese)
21. Li, D.; Zhong, Y.; Zhang, F.; Wang, L. Innovative Development of Fujian Marine Culture from the Perspective of the Maritime Community with a Shared Future. *J. Sociol. Ethnol.* **2023**, *5*, 26–32. [CrossRef]
22. Han, Q.; Tao, F.; Hong, Z.; Qin, G.; Wei, Y.; Chen, Y.; Zhou, T. Research on the spatiotemporal distribution and factors influencing intangible cultural heritage in Fujian Province from a multiscale perspective. *Herit. Sci.* **2024**, *12*, 239. [CrossRef]
23. Zhang, J.; Jiang, L.; Wang, X.; Chen, Z.; Xu, S. A Study on the Spatiotemporal Aggregation and Corridor Distribution Characteristics of Cultural Heritage: The Case of Fuzhou, China. *Buildings* **2024**, *14*, 121. [CrossRef]
24. Zhou, L.; Chang, H.T. Urban Form Analysis of Courtyard in Traditional Settlements—Case Study of Three Lanes and Seven Alleys District in Fuzhou City. *Hum. Centered Urban Plan. Des. China Vol. II Urban Des. Mobil.* **2021**, *130*, 173–192. [CrossRef]
25. Pan, Y.; He, L.L.; Shi, Y. Practice of “Living Museum” in the Traditional Architecture Culture Protection and Renewal in South Fujian. *Appl. Mech. Mater.* **2012**, *209*, 98–102. [CrossRef]
26. Shu, M.; Chen, K.; He, Y.; Wang, Y. Topical reviews of research on resilience to natural environment in Fujian traditional dwellings of China. *Environ. Res. Commun.* **2024**, *6*, 052001. [CrossRef]

27. Wang, S.P.; Xue, J.; Huang, J. The Research on South Dwellings Building-Fujian Dwellings for Example. *Appl. Mech. Mater.* **2013**, *357*, 213–218. [[CrossRef](#)]
28. Lin, M. Study on Modern Veranda Style Architecture of Yantai Mountain in Fuzhou under the Fusion of Chinese and Western Culture. *Adv. Educ. Humanit. Soc. Sci. Res.* **2023**, *4*, 239. [[CrossRef](#)]
29. Liu, Y. *Revitalizing Commercial Streets in Historical District: Evaluating a Case in Fuzhou, China*; Massachusetts Institute of Technology: Cambridge, MA, USA, 2010.
30. Huang, L.; Liu, S.; Kang, Z. The Protection of Urban Spatial Structures in Historic Cities: A Multi-Actor Perspective of the Cultural Space Construction in Fuzhou, China. *Sustainability* **2024**, *16*, 385. [[CrossRef](#)]
31. Hemmleb, M.; Weritz, F.; Maierhofer, C. Damage detection on buildings surfaces with multi-spectral techniques. In Proceedings of the CIPA 2005 XX International Symposium 2005, Torino, Italy, 26 September–1 October 2005.
32. Hemmleb, M.; Weritz, F.; Schiemenz, A.; Grote, A.; Maierhofer, C.; Wg, V. Multi-spectral data acquisition and processing techniques for damage detection on building surfaces. In Proceedings of the Image engineering and vision metrology, Dresden, Germany, 25–27 September 2006.
33. Sidiropoulou-Velidou, D.; Georgopoulos, A.; Lerma, J.L. Exploitation of thermal imagery for the detection of pathologies in monuments. In *Proceedings of the Progress in Cultural Heritage Preservation: 4th International Conference, EuroMed 2012, Limassol, Cyprus, 29 October–3 November 2012; Proceedings 4*; Springer: Berlin/Heidelberg, Germany, 2012; pp. 97–108. [[CrossRef](#)]
34. Meroño, J.E.; Perea, A.J.; Aguilera, M.J.; Laguna, A.M. Recognition of materials and damage on historical buildings using digital image classification. *S. Afr. J. Sci.* **2015**, *111*, 1–9. [[CrossRef](#)]
35. Teza, G.; Pesci, A. Geometric characterization of a cylinder-shaped structure from laser scanner data: Development of an analysis tool and its use on a leaning bell tower. *J. Cult. Herit.* **2013**, *14*, 411–423. [[CrossRef](#)]
36. Del Pozo, S.; Herrero-Pascual, J.; Felipe-García, B.; Hernández-López, D.; Rodríguez-Gonzálvez, P.; González-Aguilera, D. Multi-sensor radiometric study to detect pathologies in historical buildings. *Int. Arch. Photogramm. Remote Sens. Spat. Inf. Sci.* **2015**, *40*, 193–200. [[CrossRef](#)]
37. Riveiro, B.; Conde-Carnero, B.; González-Jorge, H.; Arias, P.; Caamaño, J.C. Automatic creation of structural models from point cloud data: The case of masonry structures. *ISPRS Ann. Photogramm. Remote Sens. Spat. Inf. Sci.* **2015**, *2*, 3–9. [[CrossRef](#)]
38. Riveiro, B.; Lourenço, P.B.; Oliveira, D.V.; González-Jorge, H.; Arias, P. Automatic morphologic analysis of quasi-periodic masonry walls from LiDAR. *Comput. Aided Civ. Infrastruct. Eng.* **2016**, *31*, 305–319. [[CrossRef](#)]
39. Jiang, W.; Zhang, F.; Lin, Q.; Li, Q. Application of Sensing Technology in the Protection of Architectural Heritage: A Review. In *Proceedings of the 2021 IEEE International Conference on Artificial Intelligence and Computer Applications (ICAICA), Dalian, China, 28–30 June 2021*; IEEE: Piscataway, NJ, USA, 2021; pp. 654–658. [[CrossRef](#)]
40. Keay, J. *China: A History*; Basic Books: New York, NY, USA, 2009.
41. Li, Z. On the Overall Protection and Cultural Heritage of Historical and Cultural Cities: Based on the Innovative Concepts and Practices of Fuzhou City, Fujian Province. *J. Fujian Inst. Social.* **2022**, *3*, 42–50. Available online: <https://chn.oversea.cnki.net/KCMS/detail/detail.aspx?dbcode=CJFD&dbname=CJFDLAST2022&filename=FJSH202203005&uniplatform=OVERSEA&v=wr9b5Q0IB8AMbV9sa0vA9HW1D0zSE6FxaqtYAbHvsL8fk7CCDWPZB2z2yVZVN94N> (accessed on 11 November 2024). (In Chinese)
42. Wu, D.W.; Zhang, X.L.; Mao, H.Y.; Wu, H. Socio-economic driving forces of land-use change in Fuzhou, the southeastern coastal area of China. In *Proceedings of the 2008 International Workshop on Earth Observation and Remote Sensing Applications, Beijing, China, 30 June–2 July 2008*; IEEE: Piscataway, NJ, USA, 2008; pp. 1–11. [[CrossRef](#)]
43. Shen, J.; Kee, G.; Shen, J.; Kee, G. Fuzhou: Re-energizing Regional Economic Development and the Changing Urban Functions. In *Development and Planning in Seven Major Coastal Cities in Southern and Eastern China*; GeoJournal Library; Springer: Cham, Switzerland, 2017; Volume 120. [[CrossRef](#)]
44. Liao, M. Integrating Into “the Belt and Road Initiative” Deeply to Promote the High-Quality Development of “Maritime Silk Road” Core Area. In *Proceedings of the 4th International Conference on Culture, Education and Economic Development of Modern Society (ICCESE 2020), Moscow, Russia, 13–14 March 2020*; Atlantis Press: Amsterdam, The Netherlands, 2020; pp. 1498–1502. [[CrossRef](#)]
45. Asghari Ilani, M.; Amini, L.; Karimi, H.; Shavali Kuhshuri, M. CNN-based Labelled Crack Detection for Image Annotation. *Preprints* **2024**, 2024051702. [[CrossRef](#)]
46. Heil, S.; Bakaev, M.; Gaedke, M. Assessing completeness in training data for image-based analysis of web user interfaces. In *Proceedings of the YSIP-3 Workshop, Stavropol and Arkhyz, Russian Federation, 17–20 September 2019*; Hölldobler, S., Malikov, A., Eds.; CEUR Workshop Proceedings: Aachen, Germany, 2019; 2500.
47. Zhang, P.; Pang, Y.; Pan, H.; Shi, C.; Huang, Y.; Wang, J. Factors Contributing to Hypoxia in the Minjiang River Estuary, Southeast China. *Int. J. Environ. Res. Public Health* **2015**, *12*, 9357–9374. [[CrossRef](#)]
48. Wu, P.; Li, S.; Wu, X. A study on the urban spatial expansion in Fuzhou, Fujian Province of China, using the SLEUTH model. In *Proceedings of the Sixth International Symposium on Digital Earth: Data Processing and Applications, Beijing, China, 9–12 September 2009*; SPIE: Washington, DC, USA, 2010; Volume 7841, pp. 554–561. [[CrossRef](#)]
49. Cheshmehzangi, A.; Tang, T. Guangdong-Fujian-Zhejiang Coastal Region: A Network Corridor Between Three Coastal Provinces. In *China’s City Cluster Development in the Race to Carbon Neutrality*; Urban Sustainability; Springer: Singapore, 2022. [[CrossRef](#)]

50. Chen, L. Research on the Development Strategy of Fuzhou Port under the Background of the “Belt and Road” Initiative. *Ind. Innov. Res.* **2018**, *8*, 25–28+35. Available online: <https://chn.oversea.cnki.net/KCMS/detail/detail.aspx?dbcode=CJFD&dbname=CJFDLAST2018&filename=CYCX201808008&uniplatform=OVERSEA&v=t04qoKMmk-fkInkIreQaBaDrb2cTb4T0pEIMto5b1VCLKo0tZAGOik9X8ULGaBL7> (accessed on 11 November 2024). (In Chinese)
51. Xu, T.; Sun, X.; Hong, H.; Wang, X.; Cui, M.; Lei, G.; Gao, L.; Liu, J.; Lone, M.A.; Jiang, X. Stable isotope ratios of typhoon rains in Fuzhou, Southeast China, during 2013–2017. *J. Hydrol.* **2019**, *570*, 445–453. [[CrossRef](#)]
52. Yang, Y.; Jiang, X.; Wang, X.; Wan, Z.; Chen, S.; Zhai, S.; He, S. Isotopic characteristics of extreme “dragon-boat water” rainfall between mid-May and mid-June in 2022 in Fuzhou, southeastern China. *J. Hydrol.* **2024**, *642*, 131870. [[CrossRef](#)]
53. Yang, L.; Yu, K.; Ai, J.; Liu, Y.; Yang, W.; Liu, J. Dominant Factors and Spatial Heterogeneity of Land Surface Temperatures in Urban Areas: A Case Study in Fuzhou, China. *Remote Sens.* **2022**, *14*, 1266. [[CrossRef](#)]
54. Fuzhou’s Climate in 2022. Available online: https://www.fuzhou.gov.cn/zgfzzt/zjrc/zrdl/202310/t20231013_4697419.htm (accessed on 31 August 2024).
55. Chen, Y.; Rui, D.; Yiqi, Z.; Shuting, W.; Siren, L. Regional Characteristics of Architectural Colors in Traditional Villages: A Case Study of Linpu Village, Fuzhou City. *J. Landsc. Res.* **2018**, *10*, 39–46. [[CrossRef](#)]
56. Chu, R. The Minnan Region of Fujian: History and Society. In *Chinese and Chinese Mestizos of Manila*; Brill: Leiden, The Netherlands, 2010; pp. 23–51. [[CrossRef](#)]
57. Ou, H.; Xiao, M. Research on Implanting the Sustainable Design in Rural Revitalization: Taking the Qianyang Village in Jin’an District, Fuzhou City as an Example. In *Proceedings of the 2nd International Conference on Architecture: Heritage, Traditions and Innovations (AHTI 2020), Moscow, Russia, 26–27 February 2020*; Atlantis Press: Amsterdam, The Netherlands, 2020; pp. 300–304. [[CrossRef](#)]
58. Lin, R.; Yang, F.; Zhang, D.; Zou, C.; Zeng, Z.; Li, X. Landscape Feature Extraction and Floristic Division of Traditional Villages in the Minjiang River Basin. *J. South Archit.* **2024**, *1*, 1–9. [[CrossRef](#)]
59. Chen, J.; Li, W. Analysis of Weathering Causes and Maintenance Suggestions of Brick Carving in Cai’s Ancient Residence. *Front. Art Res.* **2022**, *4*. [[CrossRef](#)]
60. Zheng, T. Research and Analysis of Modern Consulate Complexes-Taking Yantai Hill in Fuzhou City as an Example. *Highlights Sci. Eng. Technol.* **2023**, *79*, 63–72. [[CrossRef](#)]
61. Guan, R.; Wu, Z.; Fang, W. Characteristics and Application of Longevity Bricks in Traditional Fuzhou Dwellings. *Archit. Technol.* **2018**, *12*, 100–101. Available online: https://chn.oversea.cnki.net/KCMS/detail/detail.aspx?dbcode=CJFD&dbname=CJFDLAST2019&filename=JZY201812019&uniplatform=OVERSEA&v=qwLvFrMpeoclWgWEmcSwkU_xYtVKNZ7peCMqoYzPFUQ-nV7iudGfSpk7Db0X4ry (accessed on 11 November 2024). (In Chinese)
62. Bingwu, C. Three Lanes and Seven Alleys: An Example of a Community Museum in China’s Urban Development. *Mus. Int.* **2011**, *63*, 91–101. [[CrossRef](#)]
63. Wu, C.; Cheng, L. Research on Wall Masonry Technologies of Traditional Residences in Tukeng Village, Quangang. In *East Asian Architecture in Globalization*; EAAC; Xu, S., Aoki, N., Vieira Amaro, B., Eds.; Springer: Cham, Switzerland, 2017. [[CrossRef](#)]
64. Jin, X.; Kang, L.C.; Ou, Y.P. Ground motion attenuation relation for small to moderate earthquakes in Fujian region, China. *Acta Seismol. Sin.* **2008**, *21*, 283–295. [[CrossRef](#)]
65. Qin, X.; Wu, Y.; Lin, T.; Gao, L. Urban Flood Dynamic Risk Assessment Based on Typhoon Rainfall Process: A Case Study of Typhoon “Lupit” (2109) in Fuzhou, China. *Remote Sens.* **2023**, *15*, 3116. [[CrossRef](#)]
66. Li, Q.; Zheng, L.; Chen, Y.; Yan, L.; Li, Y.; Zhao, J. Non-destructive testing research on the surface damage faced by the Shanhaiguan Great Wall based on machine learning. *Front. Earth Sci.* **2023**, *11*, 1225585. [[CrossRef](#)]

Disclaimer/Publisher’s Note: The statements, opinions and data contained in all publications are solely those of the individual author(s) and contributor(s) and not of MDPI and/or the editor(s). MDPI and/or the editor(s) disclaim responsibility for any injury to people or property resulting from any ideas, methods, instructions or products referred to in the content.